Supplemental Information for
A Survey of Small-Scale Waves and Wave-Like Phenomena in Jupiter's Atmosphere Detected by JunoCam

Glenn S. Orton[1], Fachreddin Tabataba-Vakili[1], Gerald Eichstädt[2], John Rogers[3], Candice J. Hansen[4], Thomas W. Momary[1], Andrew P. Ingersoll[5], Shawn Brueshaber [6], Michael H. Wong[7], Amy A. Simon[8] , Michael Ravine[9], Michael Caplinger[9], Dakota Smith[10], Chloe Thepenier[11], Hamish Nicholson[12]

[1]Jet Propulsion Laboratory, California Institute of Technology, Pasadena, California, USA
[2]Independent scholar, Stuttgart, Germany
[3]British Astronomical Association, London, UK
[4]Planetary Science Institute, Tucson, Arizona, USA
[5]California Institute of Technology, Pasadena, California, USA
[6]Western Michigan University, Kalamazoo, Michigan, USA
[7]University of California, Berkeley, California, USA
[8]NASA Goddard Space Flight Center, Greenbelt, Maryland, USA
[9]Malin Space Science Systems, San Diego, California, USA
[10] National Center for Atmospheric Research, Boulder, Colorado, USA
[11]Glendale Community College, Glendale, California, USA*
[12]Harvard College, Cambridge, Massachusetts, USA

*currently at the University of California, Davis

1. Catalog of all detected waves and wave-like phenomena.

This Supplemental Information file illustrates all of the waves and wave-like phenomena, that were detected in this survey, with visual guides to their locations and properties. As in the main article, they are shown in cylindrically projected format, which were developed using the Juno SPICE trajectories and the IAU Jupiter shape model. The maps are also adjusted to compensate for illumination variations across the field and rendered in a format of 180 pixels per degree. The scale of the map excerpts shown below has been rendered to the nearest half degree. For ease of identification, the maps are stretched to the second power of the signal.

Further stretching of each color has been used in the images shown both in the primary article and those shown below. We took a radiometric point at or near the minimum of the radiance histogram and set it to zero and a radiometric point at or near the maximum of the radiance histogram and set it to 255. *No attempt was made to make color or hue of the map excerpts look "Jupiter-like."* Some mitigation of this extreme approach was necessary in cases when strong camera artefacts or otherwise strong coloration resulted that would distract the reader from the wave patterns we intended to illustrate. When necessary, other approaches to illustrating the waves were used, such as unsharp masking; those instances are noted in the figure captions.

White lines or arrows are used to indicate most of the waves we detect in each figure. The figure captions refer to these as grids. For some images, the waves are so abundant in the field that not all were identified, because the grids themselves would obscure many of the waves.

Figure numbers are identified using the perijove (PJ) number and a short version of the image number within the perijove, with features shown chronologically – typically following northern to southern latitudes, following the sequence of an image set. Full image file identifiers are also provided, as shown for these images on the Mission Juno web site metadata files (for example, see https://www.missionjuno.swri.edu/junocam/processing?source=all&ob_from=&ob_to=&perpage=16.)
So the first image, from perijove 1, is titled Figure PJ01_6171, whose image file is JNCE_2016240_00C06171_V01.

There are instances in which the same region is observed in more than one image. For economy of space, we illustrate only a single example here.

In the interest of thoroughness, we include several examples of repeated patterns whose identification as waves or even wave-like might be marginal. We note these in the captions and suggest that this image set as a whole might generate discussions beyond the otherwise narrow scope of this article. We identify the context of the region illustrated using traditional nomenclature (see Rogers 1995).

No images were taken during PJ2 due to a spacecraft safing event, and the limited observations by JunoCam that were possible during PJ19 were insufficient to resolve any waves or wave-like features.

Here and in the main article the term 'PJ' refers to each orbit's "perijove", or closest approach to Jupiter, when is when all JunoCam images of relevance were made.

Additional contextual information about all of the JunoCam images from which these observations were made are available in summary reports and images by co-author J. Rogers for
PJ1-PJ10 at https://britastro.org/node/7982,
PJ11-PJ17 at https://britastro.org/node/12137, and
PJ18-onward at https://britastro.org/node/17650.

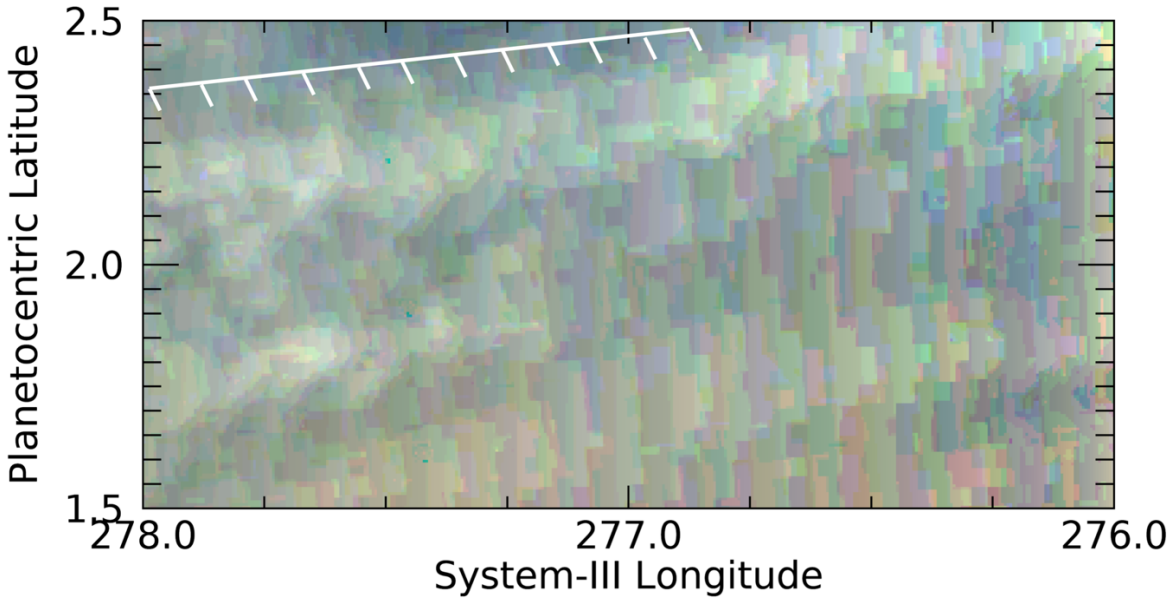

Figure PJ01_6171. JNCE_2016240_00C06171_V01. Note that PJ01 was a test PJ, not a science PJ, and many JunoCam images had image-compression artefacts, including this one. Nonetheless, a regular pattern of waves can be identified in all three colors. A repeatable pattern in the Equatorial Zone is indicated by the white grid.

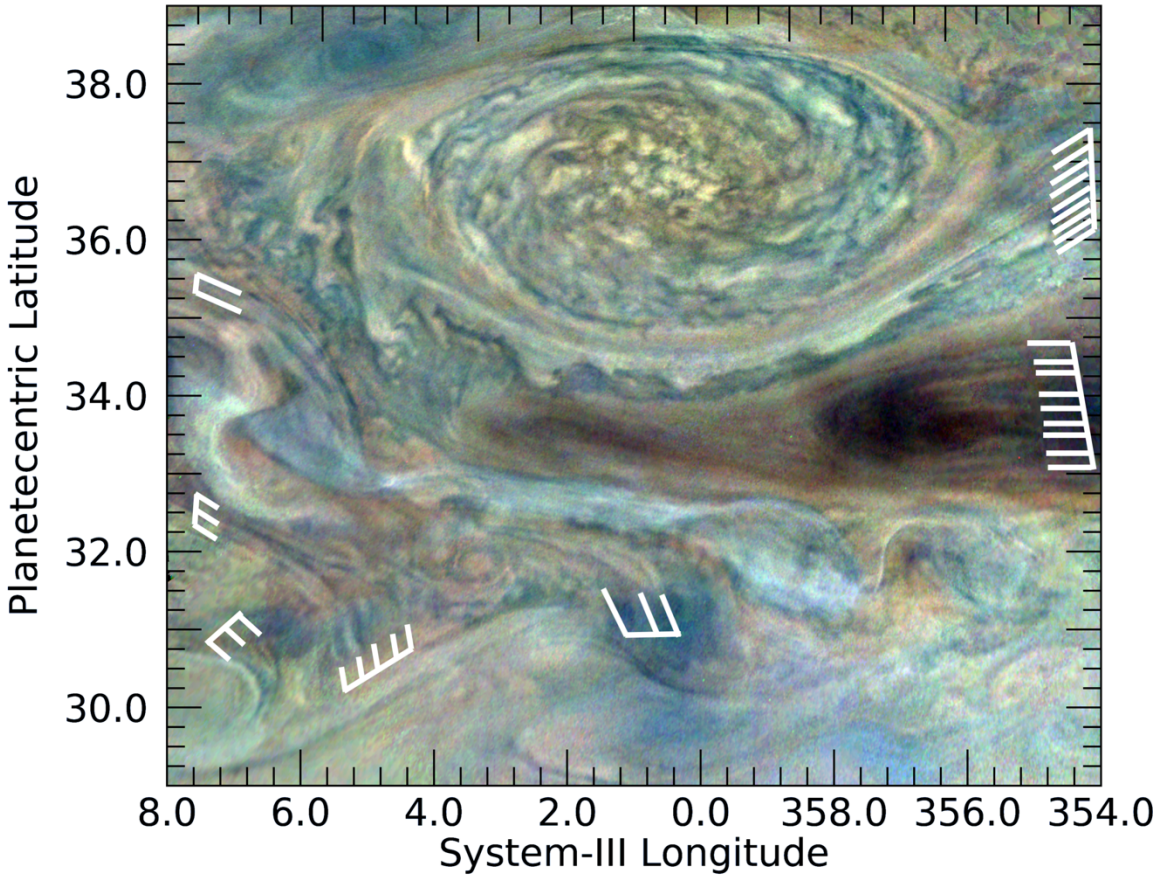

Figure PJ03_107. JNCE_2016346_03C00107_V01. There are many linear and curved streaks in this region of Jupiter that are associated with flow to the south of a reddish anticyclonic vortex, identified in co-author Rogers' reports as 'NN-LRS-1' (for North-North Little Red Spot #1). Some of the curved feature in the mid-to-lower left of this figure rise above the background cloud deck, as shown by the shadows they cast. Wave-like lines extend out from the NN-LRS-1 to its southeast and parallel some in the North North Temperate Belt (NNTB), the dark region to its south. The lighter region to the south of the NNTB is the northern component of the North Temperate Zone (NTZ).

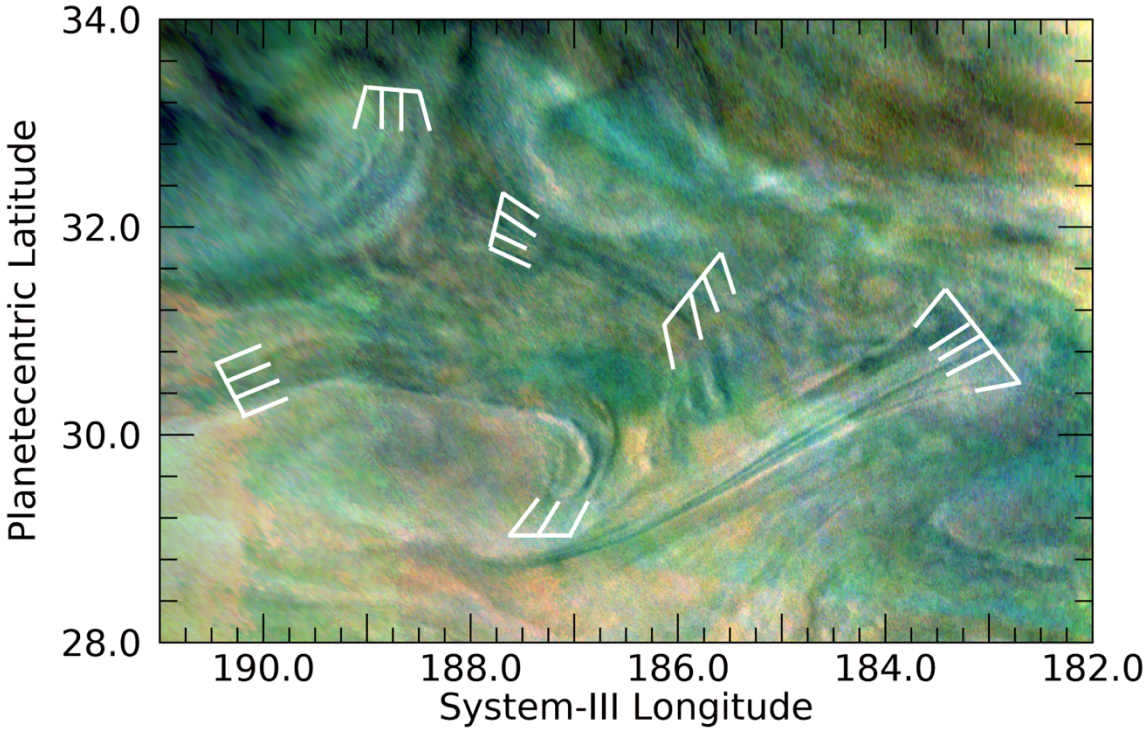

Figure PJ03_109a. JNCE_2016346_03C00109_V01. There are curved and linear cloud banks, identified by their shadows, associated with an anticyclonic vortex (lower left) in the North Temperate Zone. They are part of a circulation around the vortex, which is the central one of three appearing in Image 109; part of the eastern one can also be seen in this figure (lower right). These vortices are associated with the North North Temperate Belt south (NNTBs) jet at 31.7°N and may be moving with it. Other associated flow lines are also indicated. The color scheme has been modified to minimize artefactual green and red colored bands; in doing so, some whitish-colored haze bands can also be seen that may be associated with the flow.

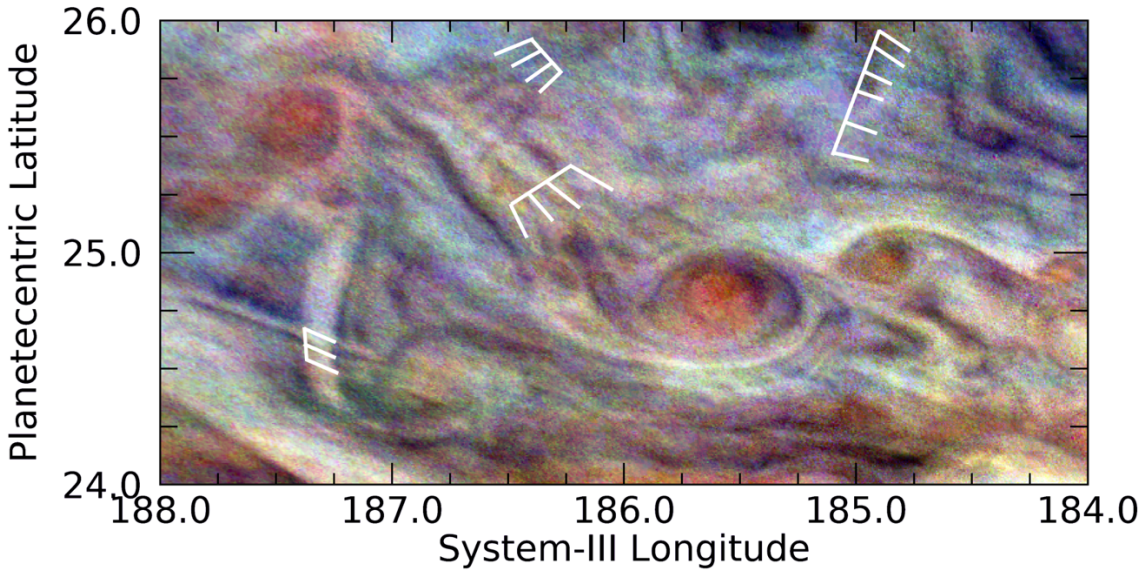

Figure PJ03_109b. JNCE_2016346_03C00109_V01. This figure illustrates many cloud features that include several sets of what appear to be flow lines between and around small anticyclonic vortices that appear reddish in the northern component of the North Temperate Belt (NTBn). The NTB was very turbulent at the time of these observations, following a great NTB disturbance in the preceding months (see Sanchez-Lavega et al. 2017). A triplet of short, dark bands in the top left of this figure can be seen lying across longer bands that appear to be flow lines.

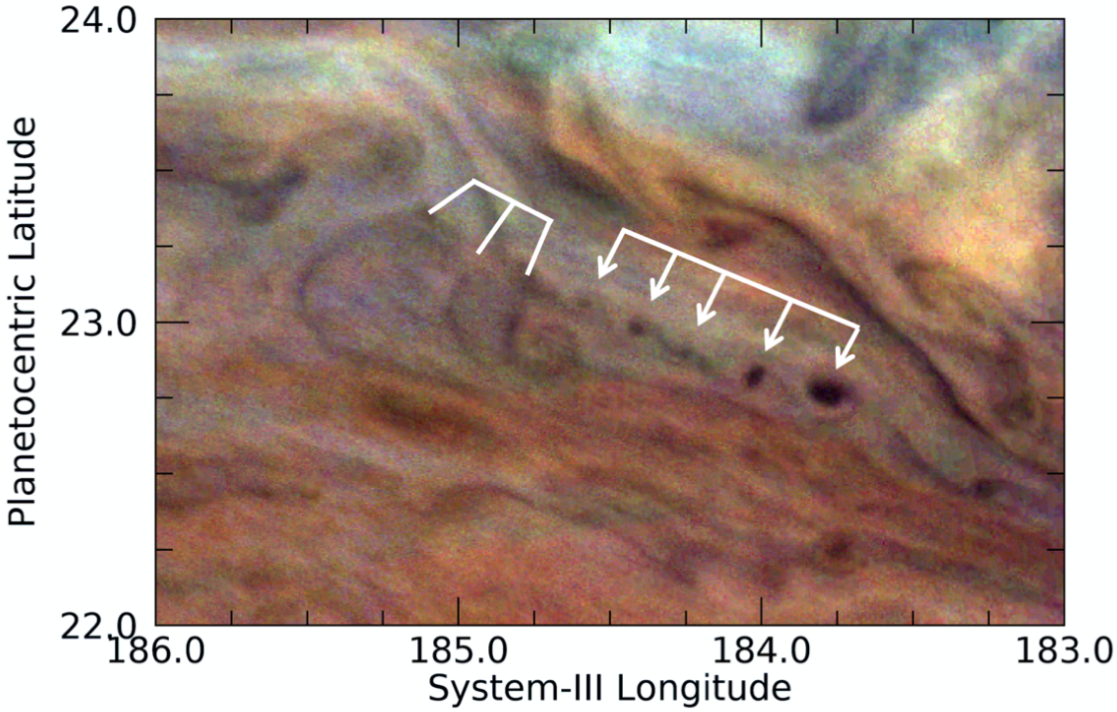

Figure PJ03_109c. JNCE_2016346_03C00109_V01. Three curved wavefronts are indicated. The arrows point to an unusual series of relatively dark circular features, possibly connected dynamically to the wavefronts, because they continue in the same direction and have roughly the same wavelength. These features are located near the boundary between the turbulent northern component and the smooth, orange southern component of the North Temperate Belt.

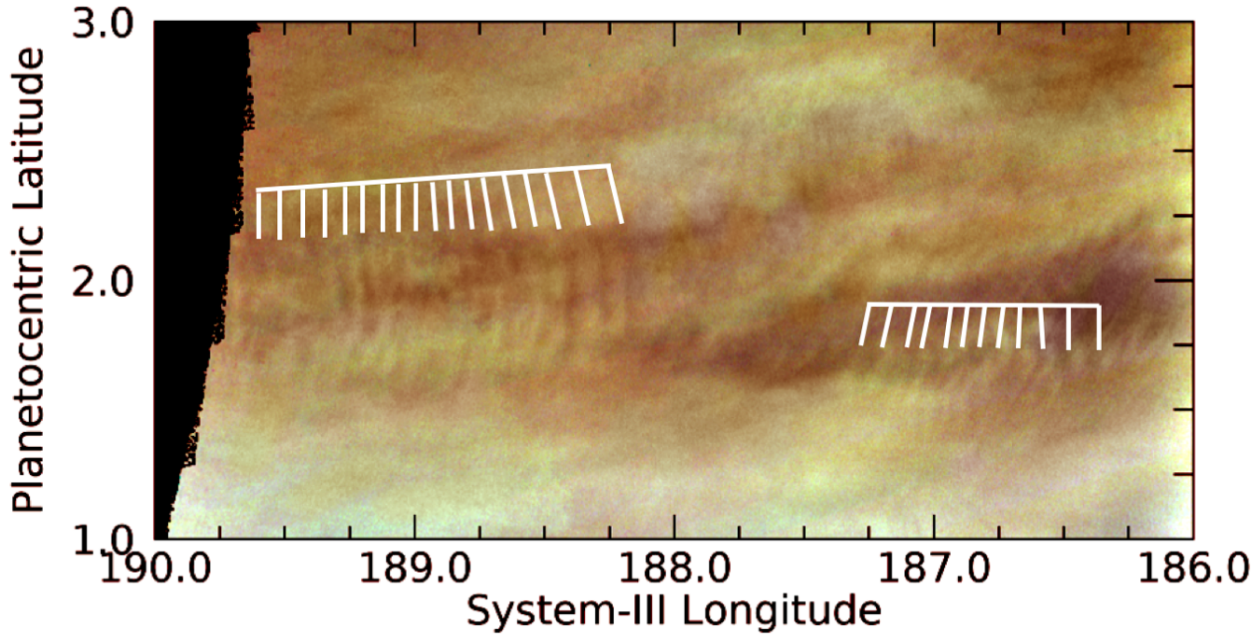

Figure PJ03_111a. JNCE_2016346_03C00111_V01. Two sets of waves are detectable in this figure. In order to see both sets of waves where the background illumination is strongly varying, adjusted histogram equalization has been applied to the image. Some image blockiness due to compression artifacts remains. Nevertheless, this is one of our clearest illustrations of wave fronts that are orthogonal to the direction of the wave train.

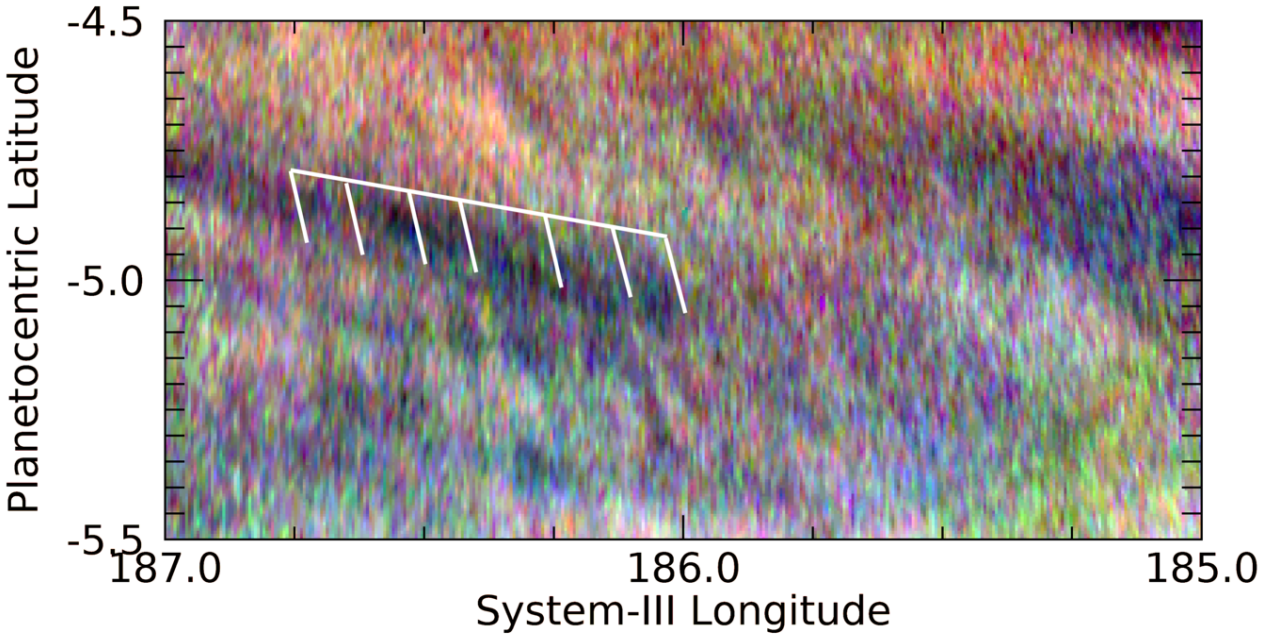

Figure PJ03_111b. JNCE_2016346_03C00111_V01. Some very subtle waves in the Equatorial Zone are detectable above the noise in this image.

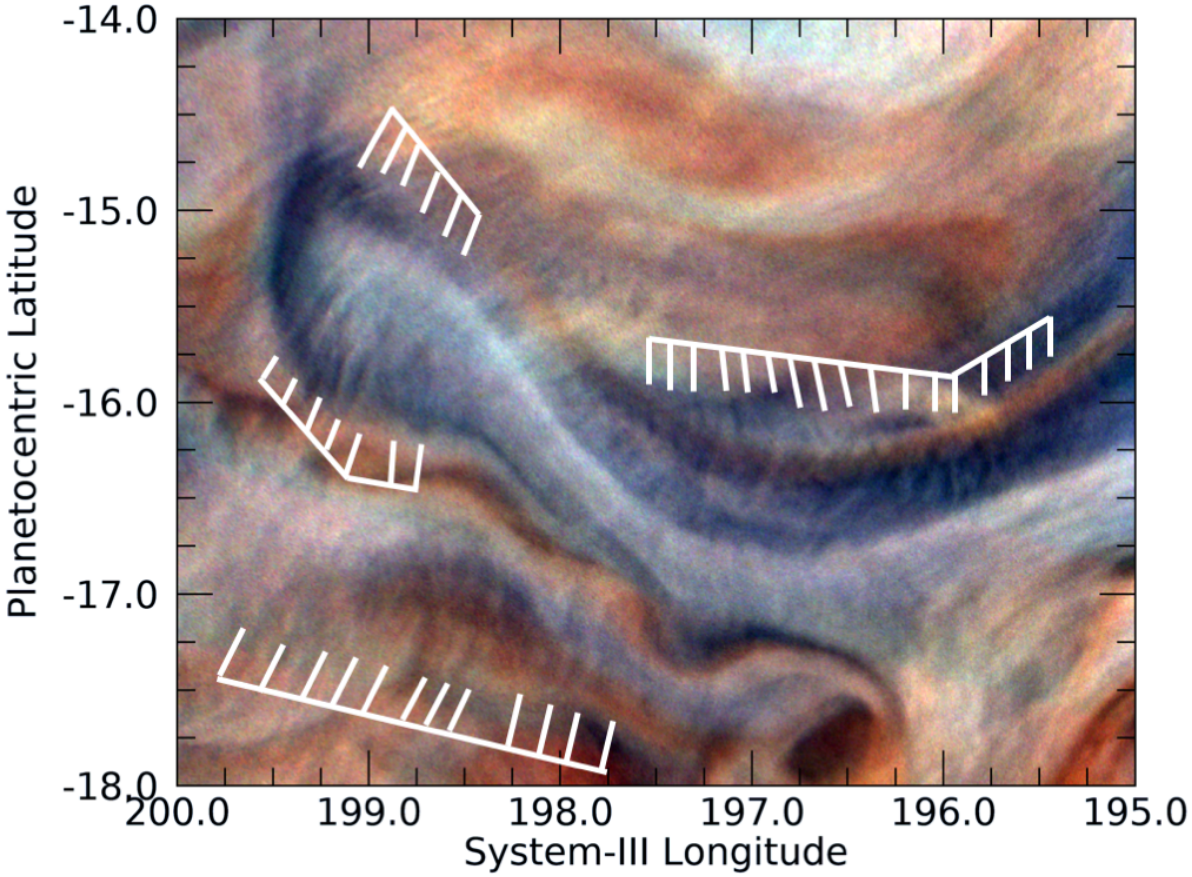

Figure PJ03_114. JNCE_2016346_03C00114_V01. Wave-like features appear along and extending from the curves periphery of this darker feature in the South Equatorial Belt (SEB).

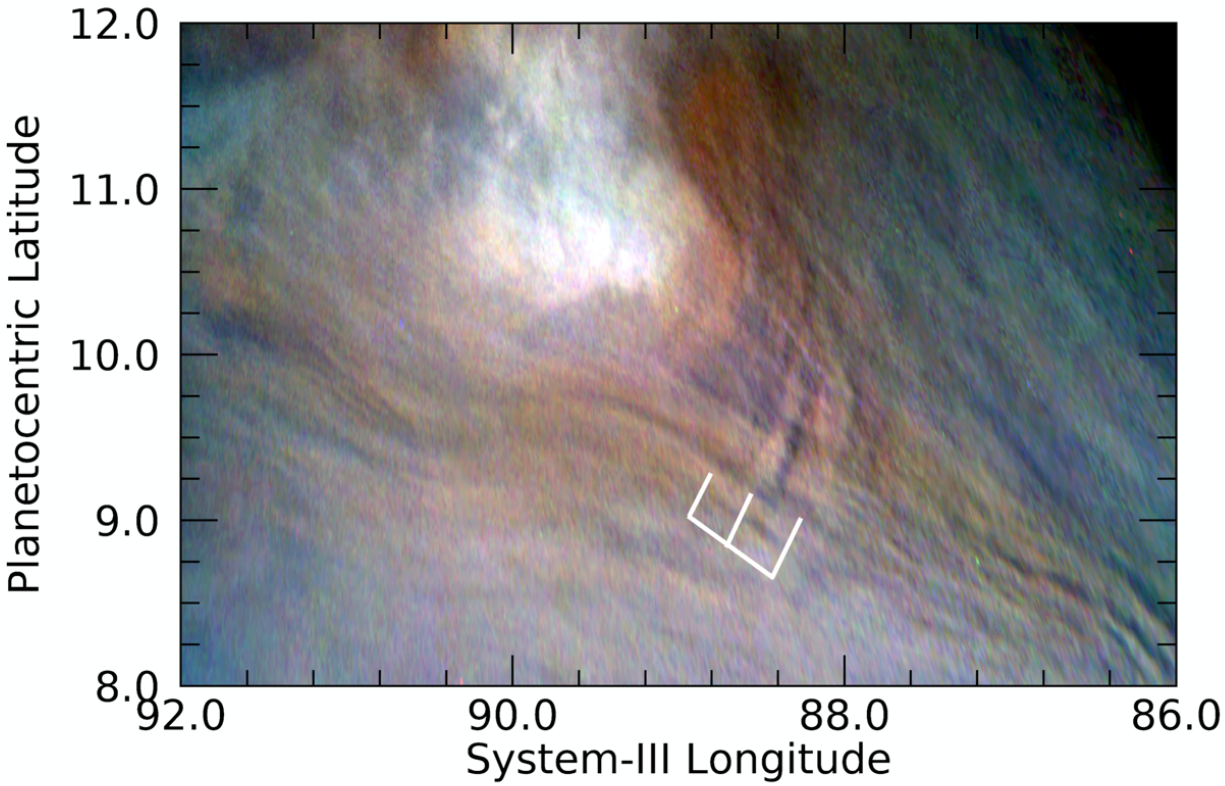

Figure PJ04_102. JNCE_2017033_04C00102_V01. Waves are prominent topographically from their prominent shadows, appearing orthogonal to the dark and light streaks that are presumed to be lines of flow that are aligned with the cyclonic wind gradient in the North Equatorial Belt (NEB). The 'flow lines' appear to go not only around the bright feature, which is likely to be a convective plume, but over it. Thus, the prominent orthogonal waves are most likely to be only example of a true downslope lee wave we have detected in the atmosphere of Jupiter from JunoCam.

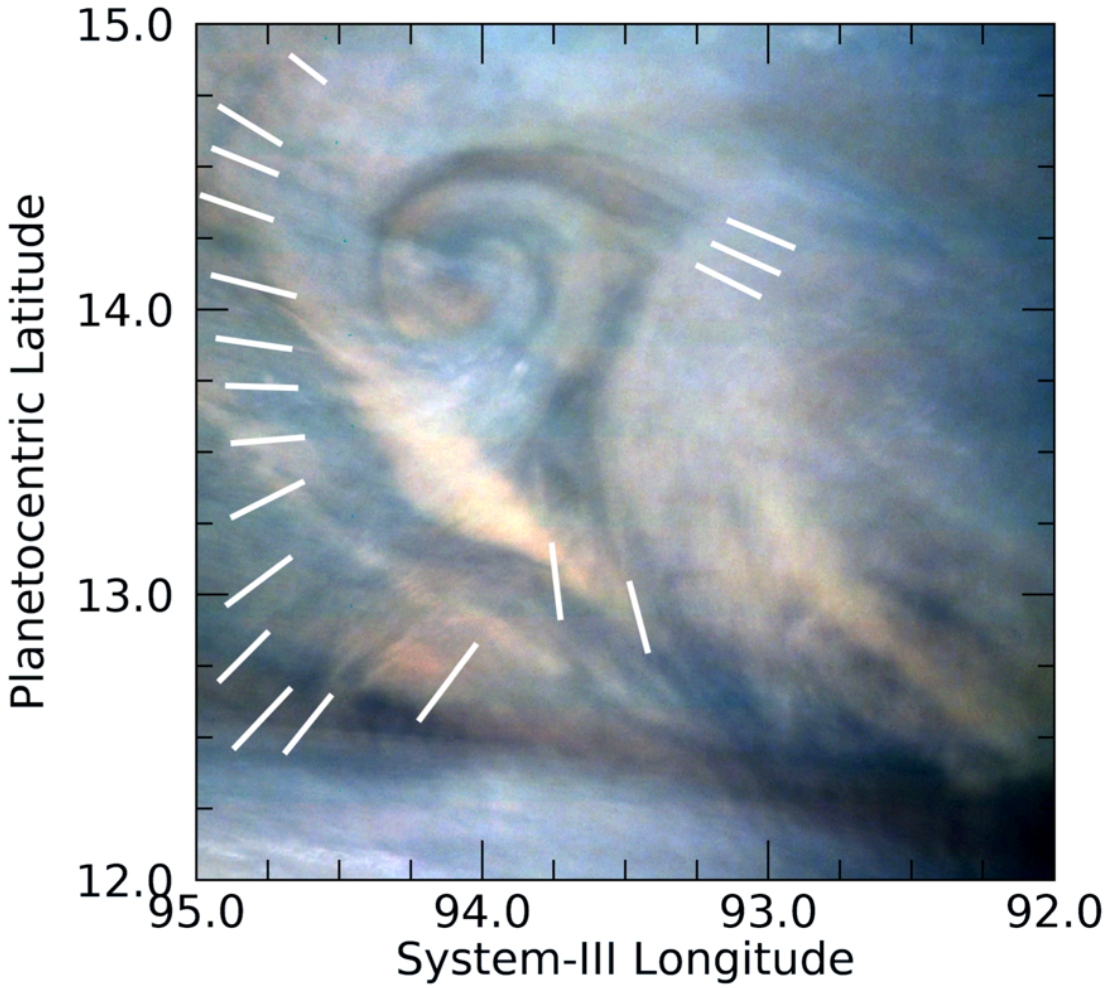

Figure PJ04_103a. JNCE_2017033_04C00103_V01. Wave fronts are apparent in the periphery of a remarkable cyclonic spiral. The spiral is a bright feature in the complex system of disturbances ('rifts') in the North Equatorial Belt.

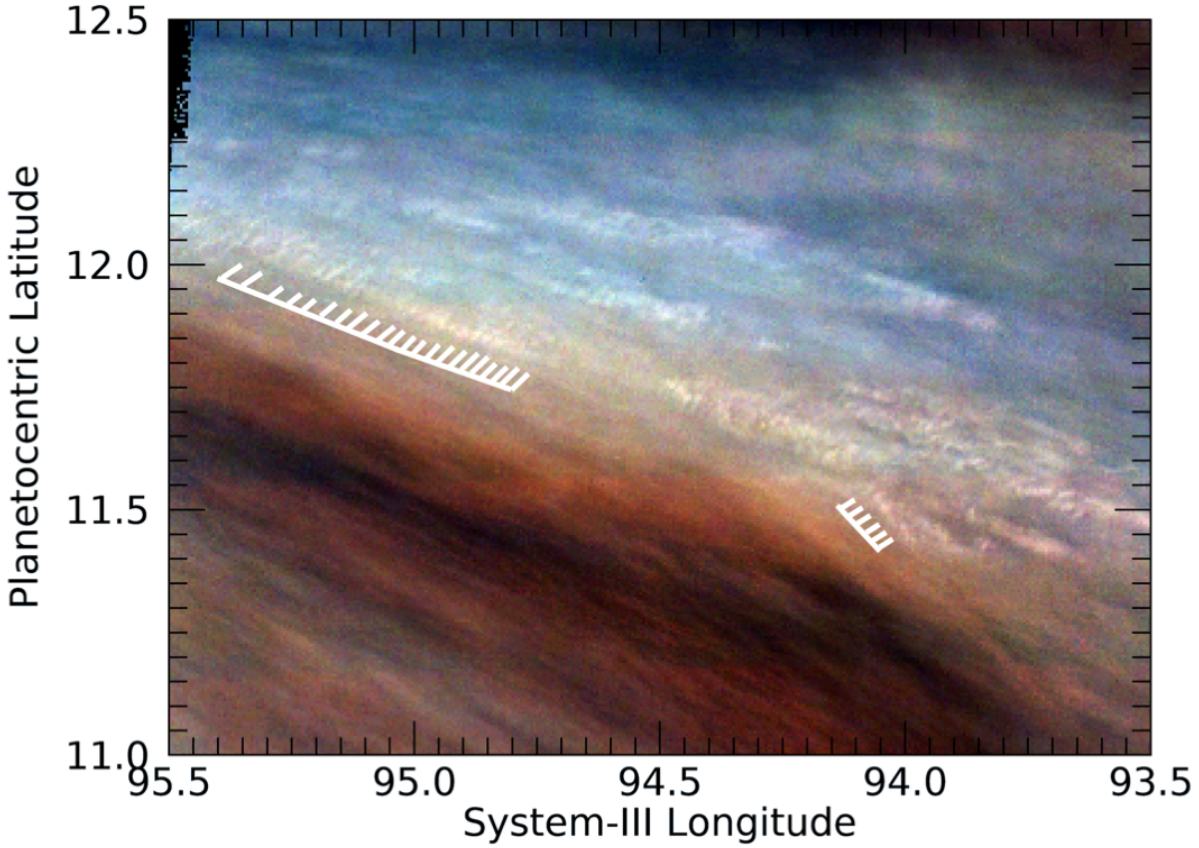

Figure PJ04_103b. JNCE_2017033_04C00103_V01. This figure reveals extensive wave packets controlling small, bright cloud features in a bright patch of the complex 'rift' system in the North Equatorial Belt (NEB). White grids identify packets in which the individual cloud features are resolved clearly. These packets are aligned with the cyclonic wind gradient across the NEB and roughly orthogonal to the waves; the wind gradient is also suggested by many faint striations with similar alignment in the surrounding bright area and in the dark brown area to the south (see the report on JunoCam images from PJ4 by co-author Rogers at https://britastro.org/sites/default/files/Juno-PJ4_Report_JHR_0.pdf).

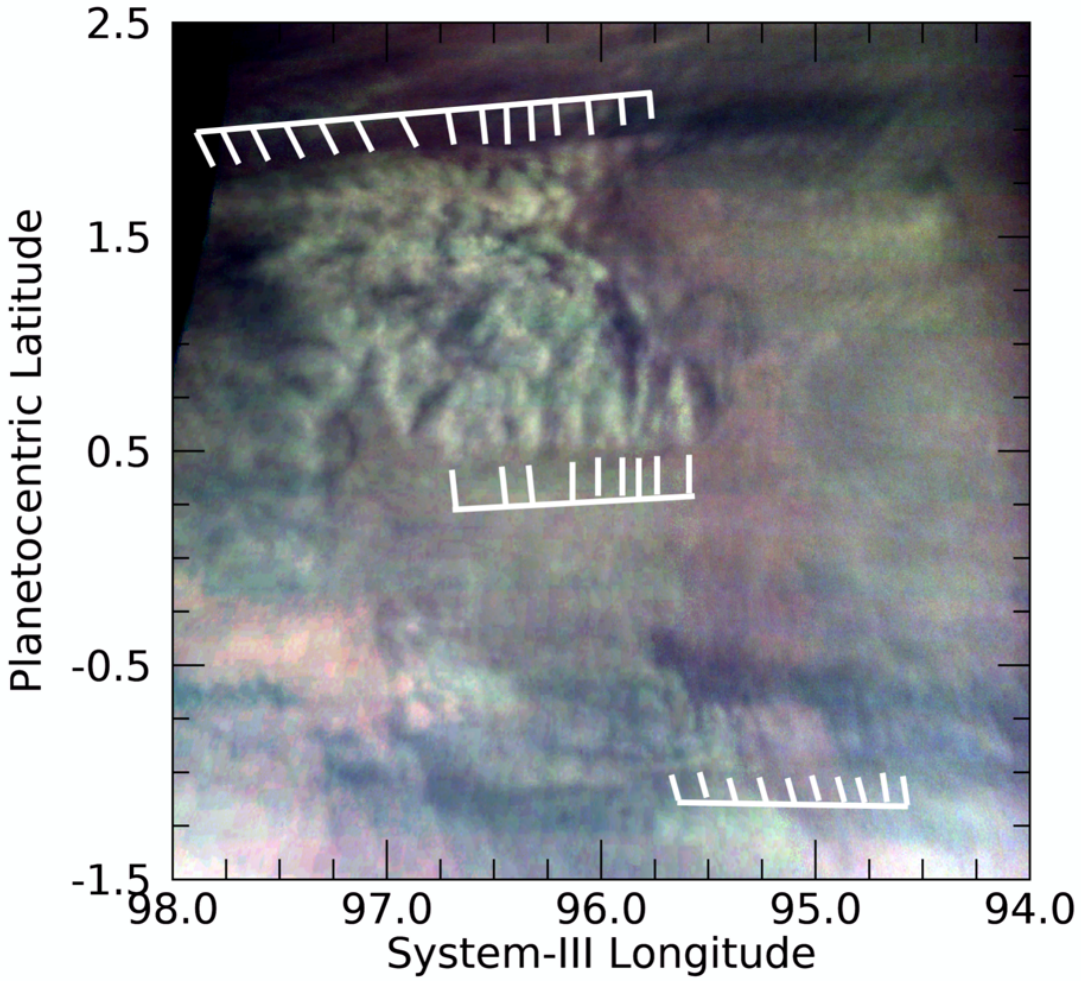

Figure PJ04_104a. JNCE_2017033_04C00104_V01. Multiple sets of wave trains can be identified in this image of a region in the EZ. (Note: this color scheme was adopted to minimize the appearance of artefactual green and red stripes across the frame, although a residual still remains.)

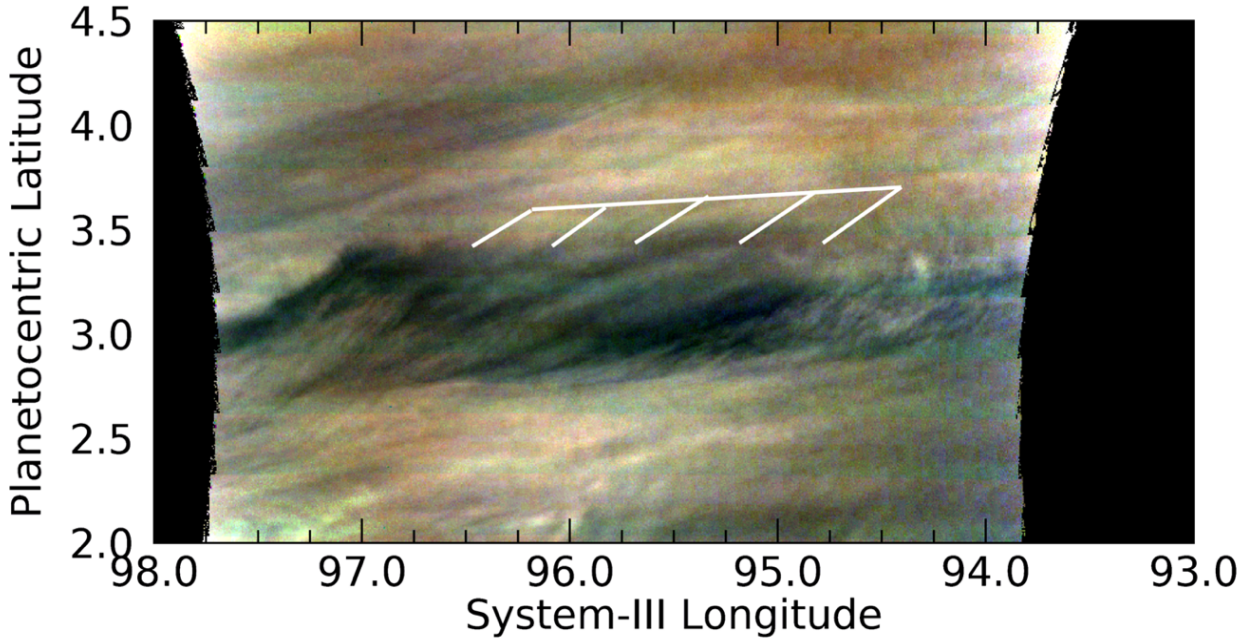

Figure PJ04_104b. JNCE_2017033_04C00104_V01. Long, wave-like patterns can be seen in this image overlapping a darker feature in the Equatorial Zone.

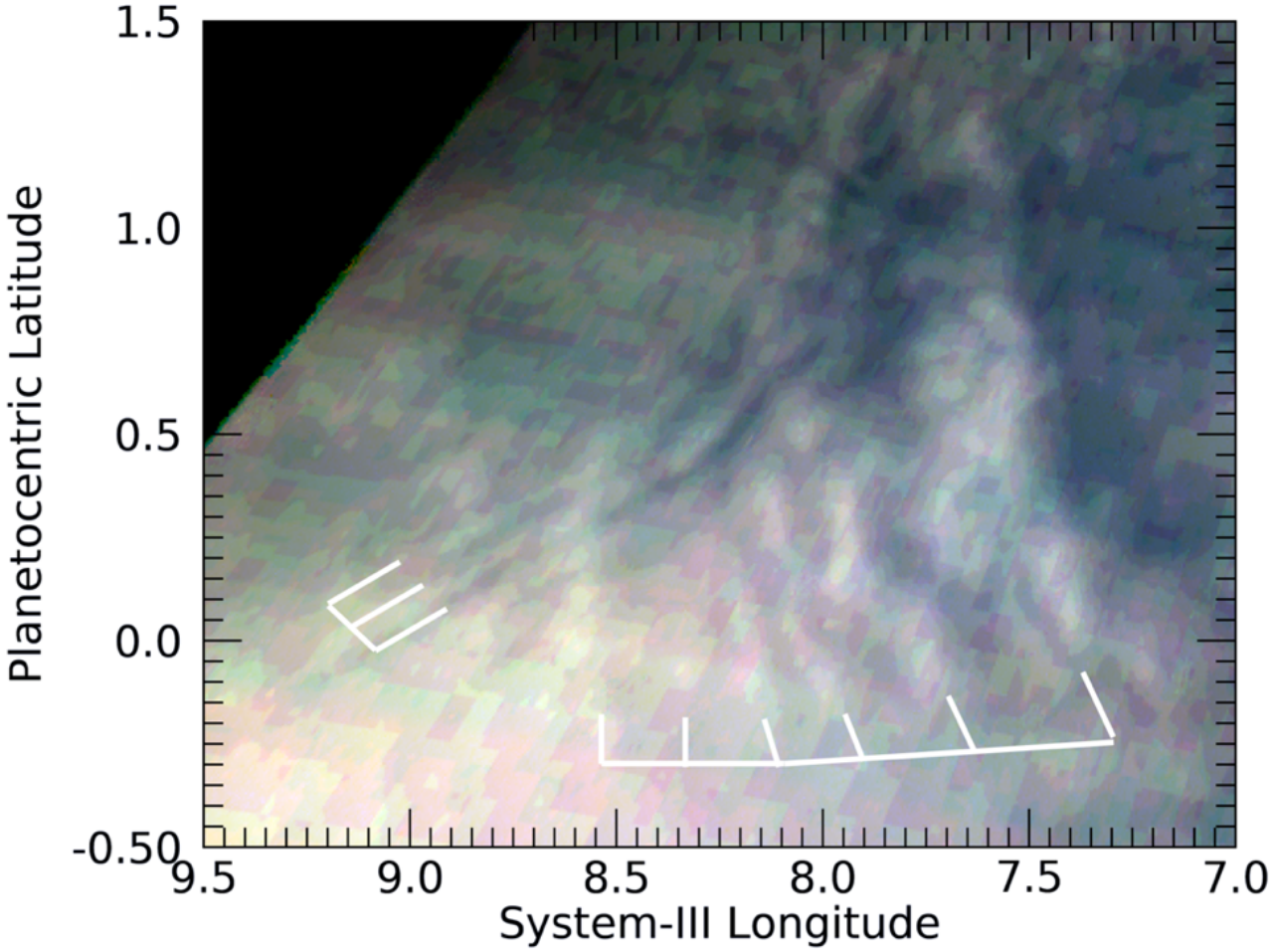

Figure PJ05_107a. JNCE_2017086_05C00107_V01. Two sets of overlapping waves are detected in the Equatorial Zone, both with wavefronts that are longer than the wave packets. (Note: as in Figure PJ04_104a, this color scheme was adopted to minimize the appearance of artefactual green and red stripes across the frame.)

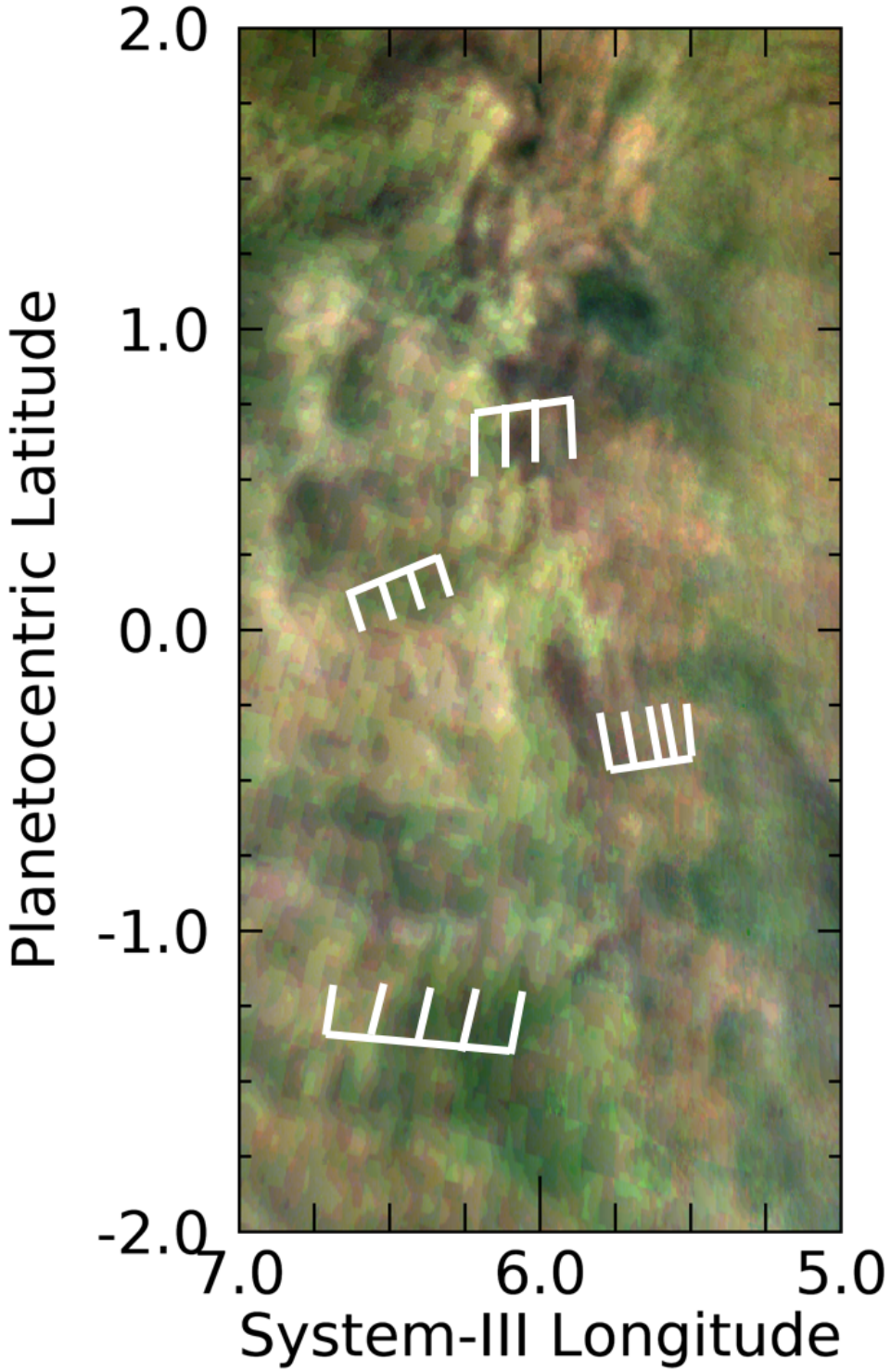

Figure PJ05_107b. JNCE_2017086_05C00107_V01. Several sets of waves can be detected in this area of the Equatorial Zone.

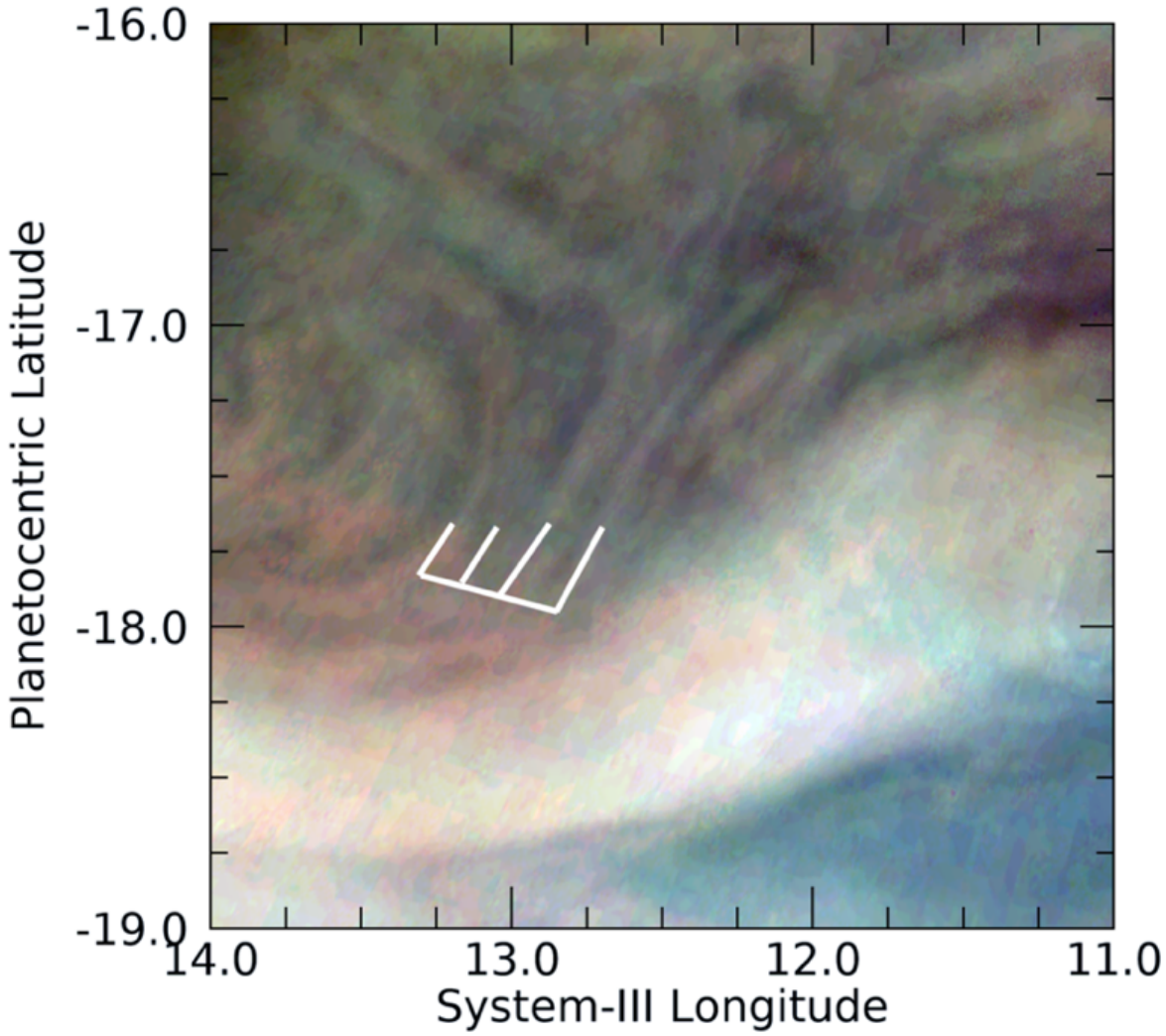

Figure PJ05_108. JNCE_2017086_05C00108_V01. Parallel bands, likely representing a flow pattern, are located in a pale strip of the southern component of the South Equatorial Belt (SEBs). They are located between a weak cyclonic eddy on the left and a bright wave-like streak aligned with the SEBs retrograde jet, running near the bottom edge of the figure. These bands are similar to those in the Figure PJ03_109b.

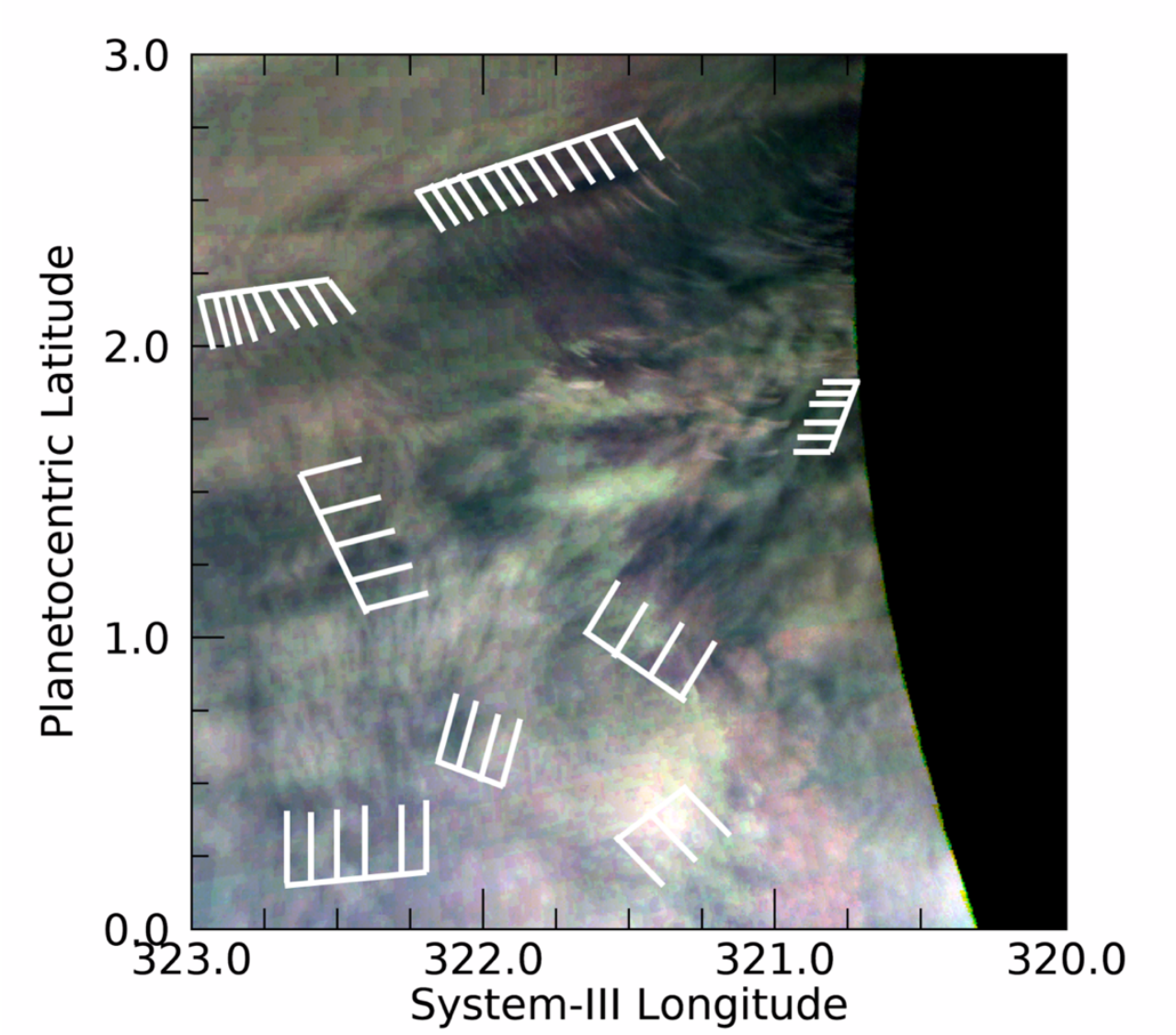

Figure PJ06_115. JNCE_2017139_06C00115_V01. This figure illustrates multiple sets of often overlapping and orthogonal waves present in the Equatorial Zone. (Note: as in Figures PJ04_104a and PJ05_107a, this color scheme was adopted to minimize the appearance of artefactual green and red stripes across the frame.)

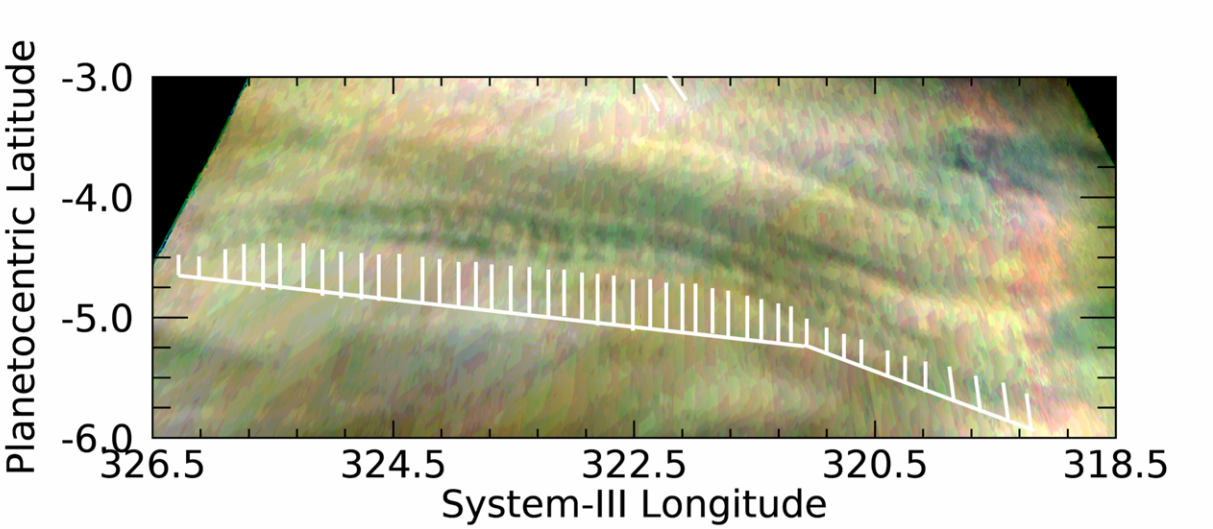

Figure PJ06_115. JNCE_2017139_06C00115_V01. This figure illustrates a series of waves appearing most prominently as "knots" on a narrow, linear bright cloud bank in the Equatorial Zone.

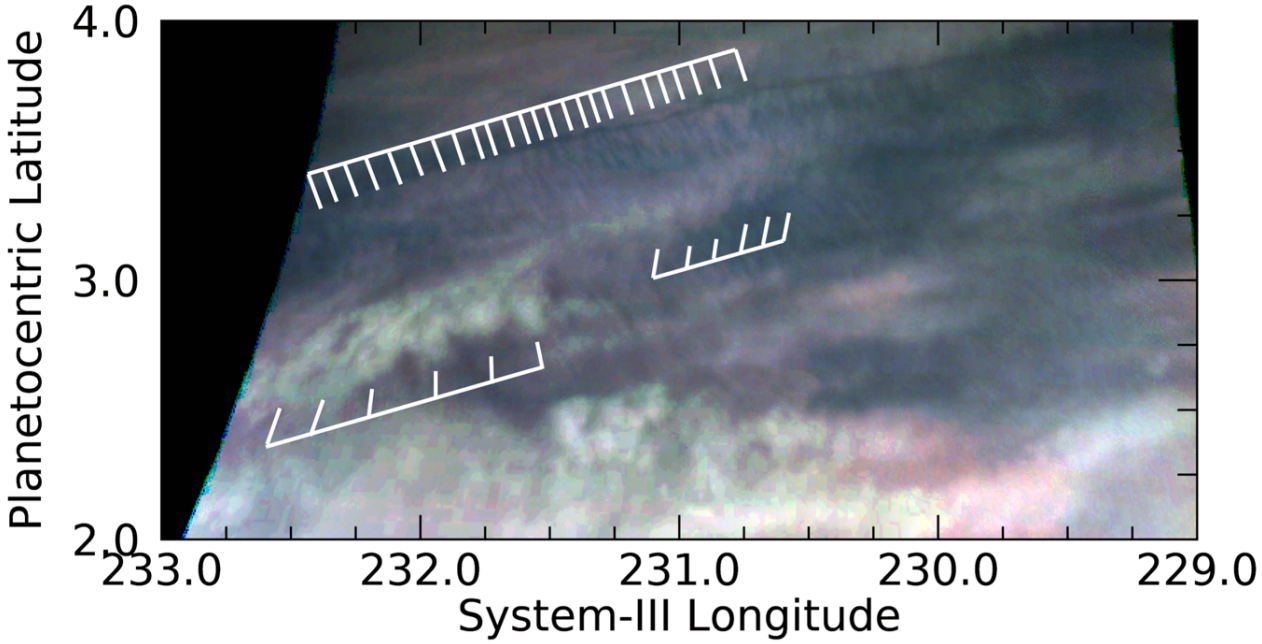

Figure PJ07_57. JNCE_2017192_07C00057_V01. Several wave packets can be identified in this area of the Equatorial Zone.

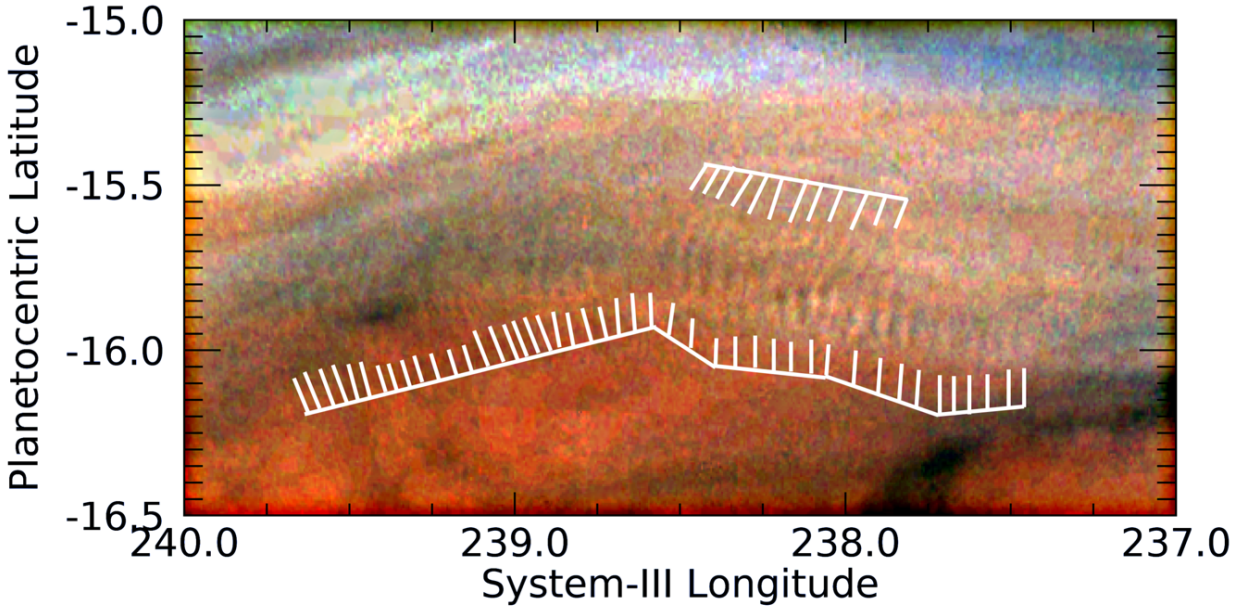

Figure PJ07_60. JNCE_2017192_07C00060_V01. This shows two interfering sets of waves in the northern part of the GRS. This is the same wave feature as shown by Sanchez-Lavega et al. (2018) in their Figure 8. Besides being color-stretched, this image was also unsharp-masked

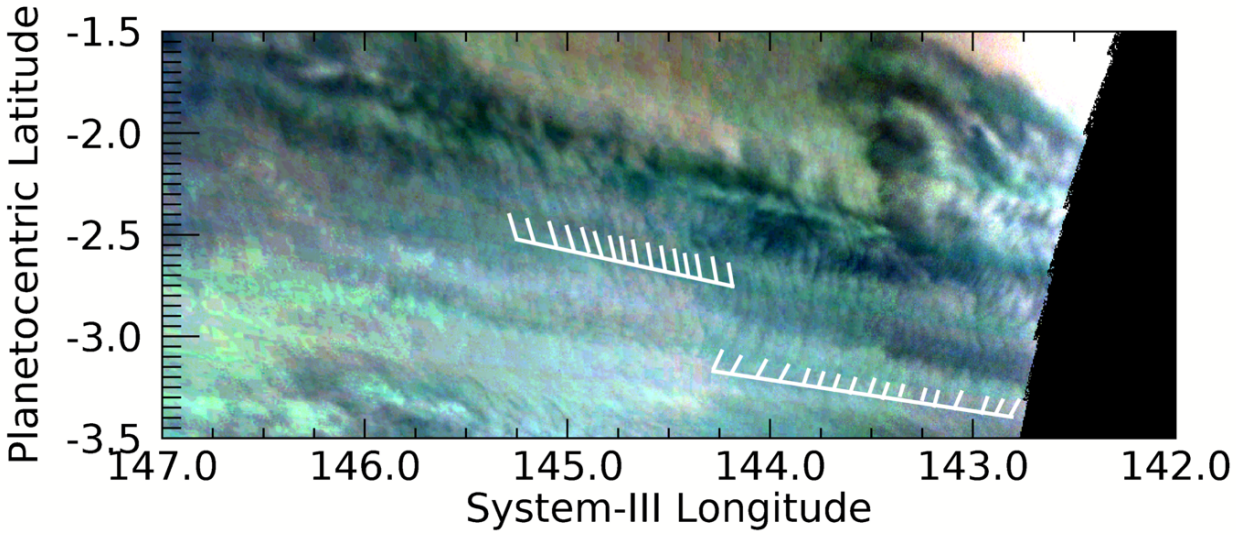

Figure PJ08_116a. JNCE_2017244_08C00116_V01. This image shows evidence for multiple sets of waves, the most prominent two of which are illustrated by the grids.

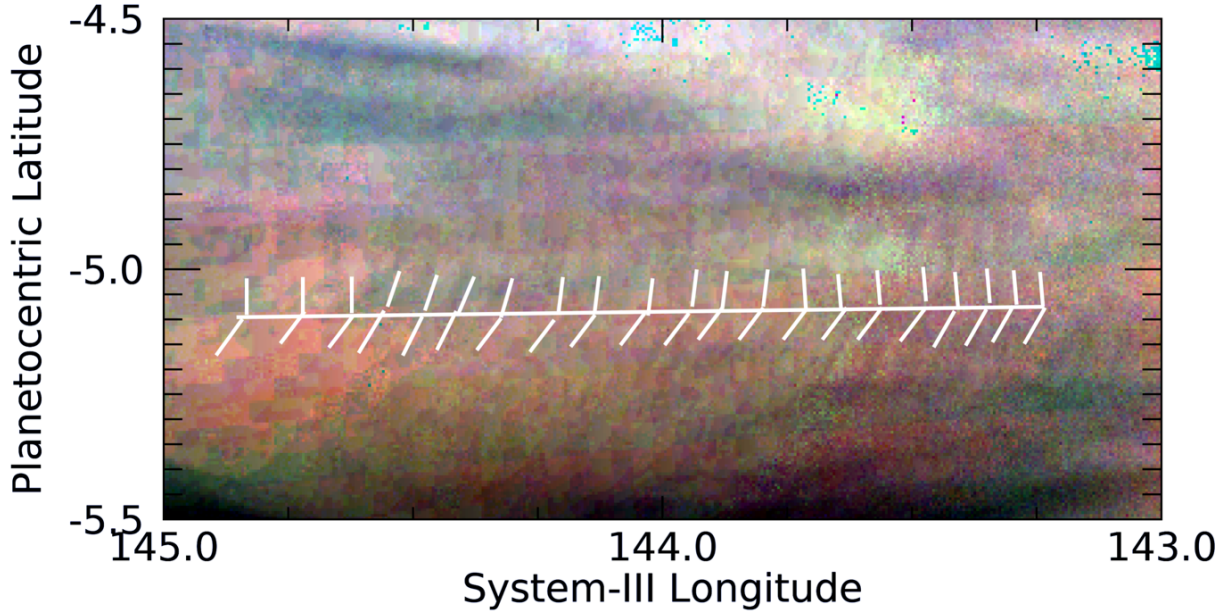

Figure PJ08_116b. JNCE_2017244_08C00116_V01. Two tilts appear to be the characteristic of these very subtle waves that are just detectable above the compression noise of this image.

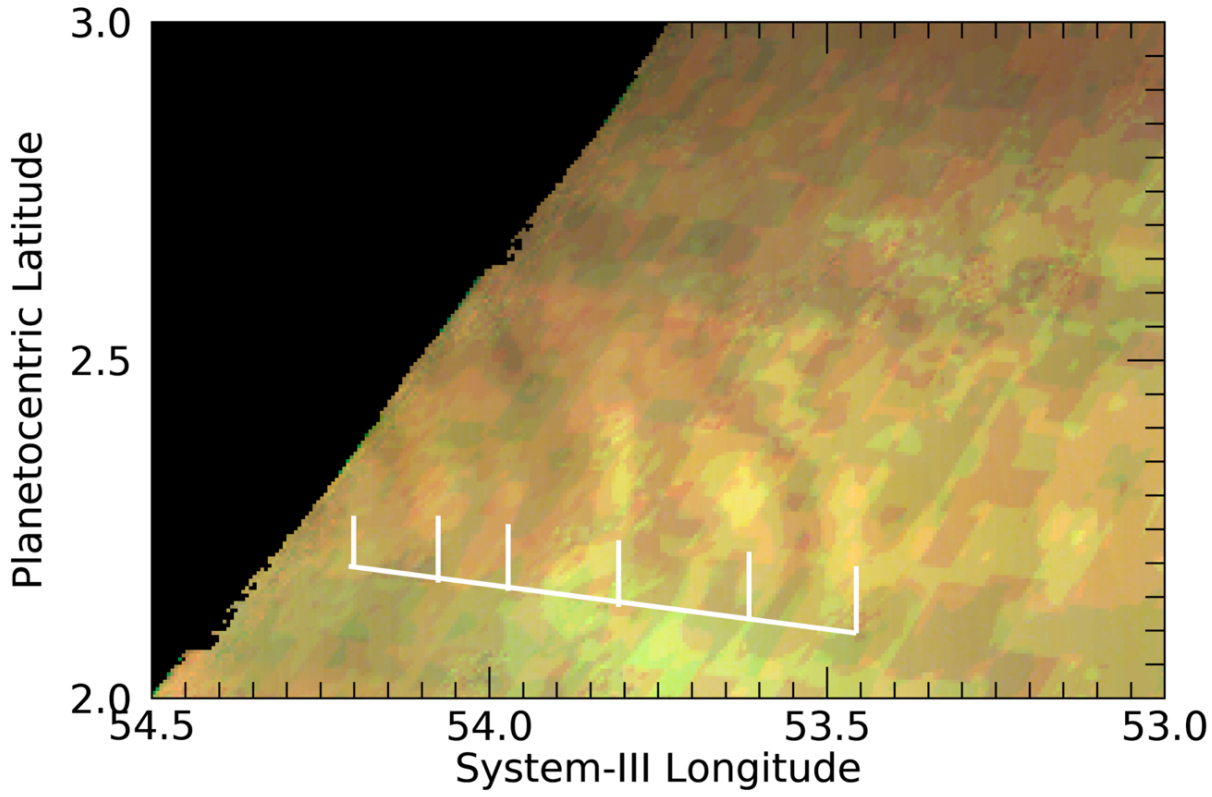

Figure PJ09_85. JNCE_2017297_09C00085_V01. Waves can be detected above the compression noise of this image.

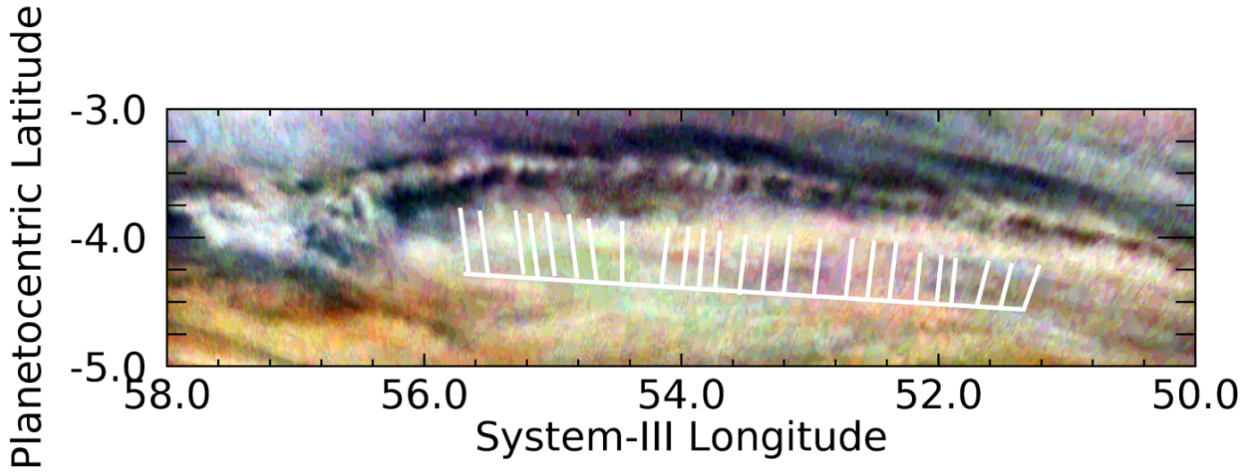

Figure PJ09_88. JNCE_2017297_09C00088_V01. The grid points to discrete white clouds that appear like 'knots' in the narrow 'rope' that forms a series of waves that follow a long, curved wave packet.

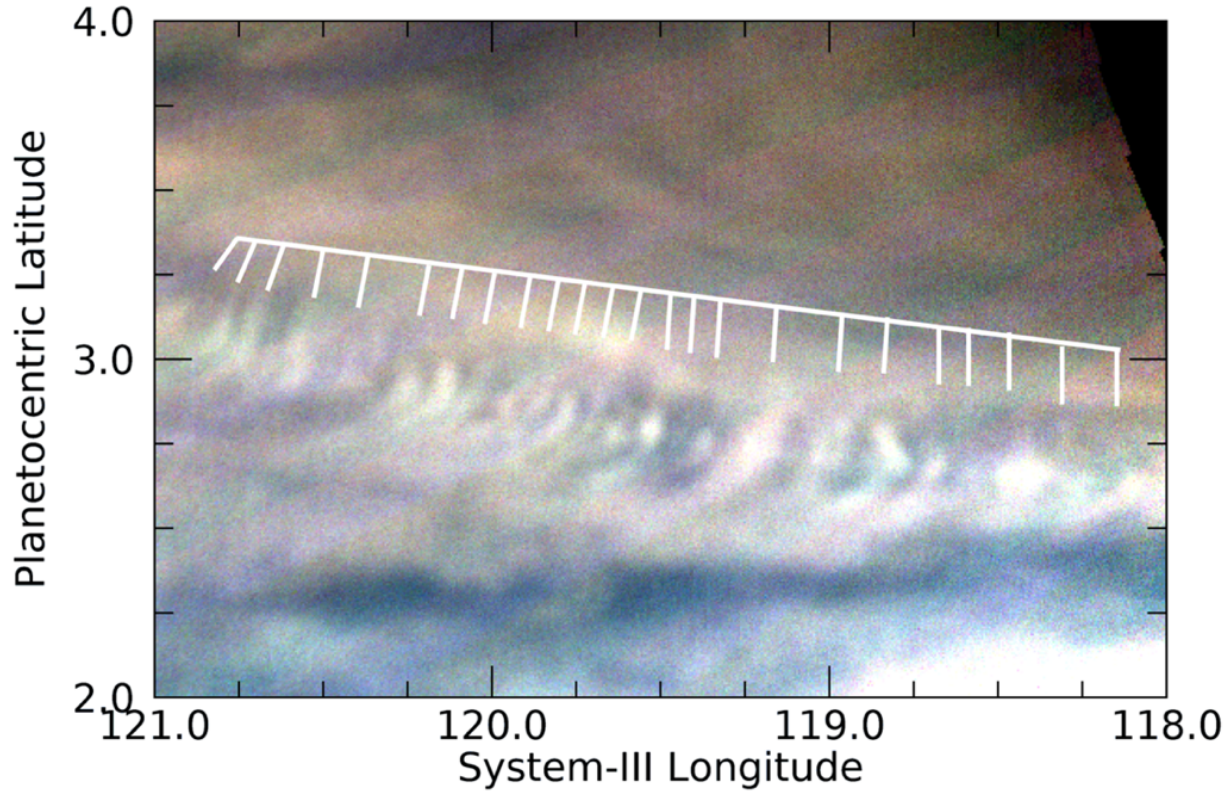

Figure PJ10_28b. JNCE_2017350_10C00028_V01. A series of discrete, bright cloud features comprises a wave packet in the Equatorial Zone. Unlike the wave packet shown in Fig. PJ09_88, there is not such an obvious bright 'line' connecting them

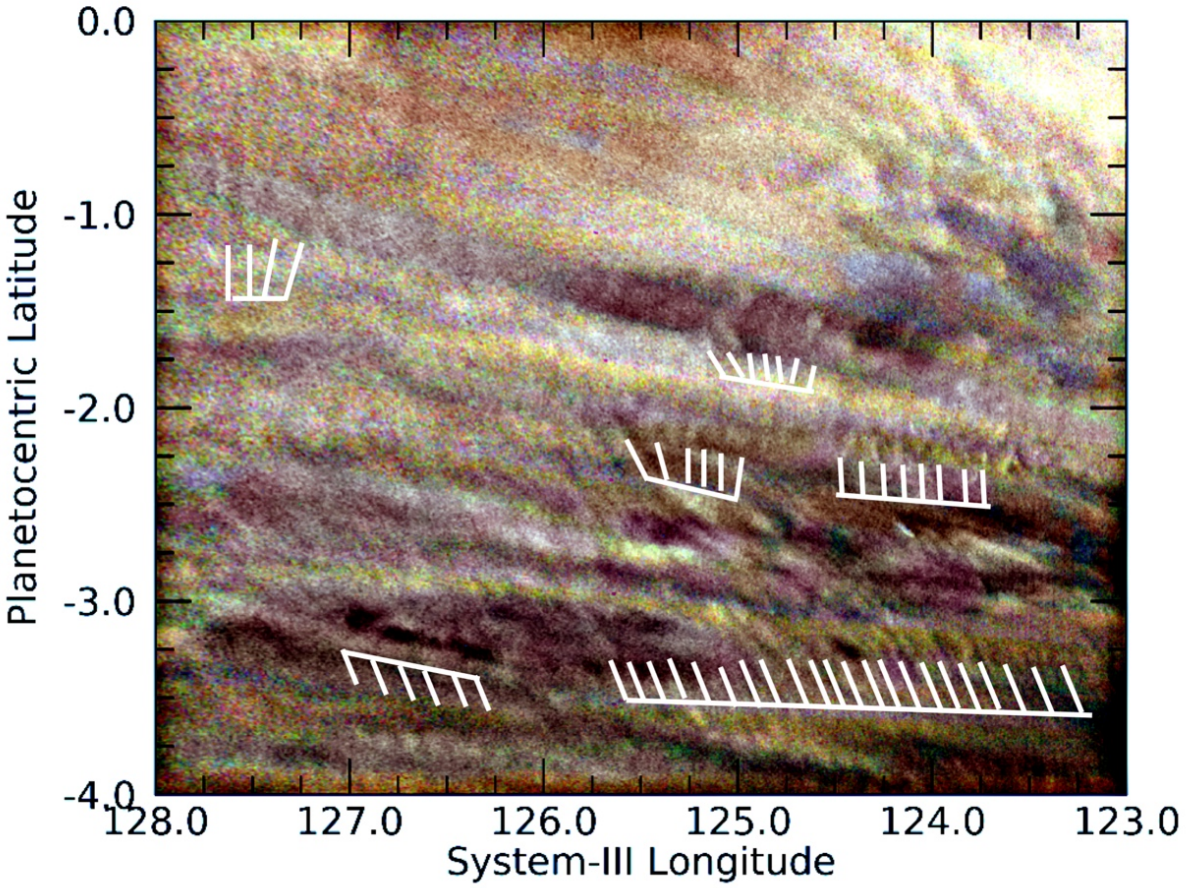

Figure PJ10_30a. JNCE_2017350_10C00030_V01. Several wave trains are detectable above the noise in this image, some of which are indicated by the white grid lines. We have numerically suppressed artificial colored striping across the field. (In order to show waves in both the light and dark regions of this image, we have used unsharp masking.)

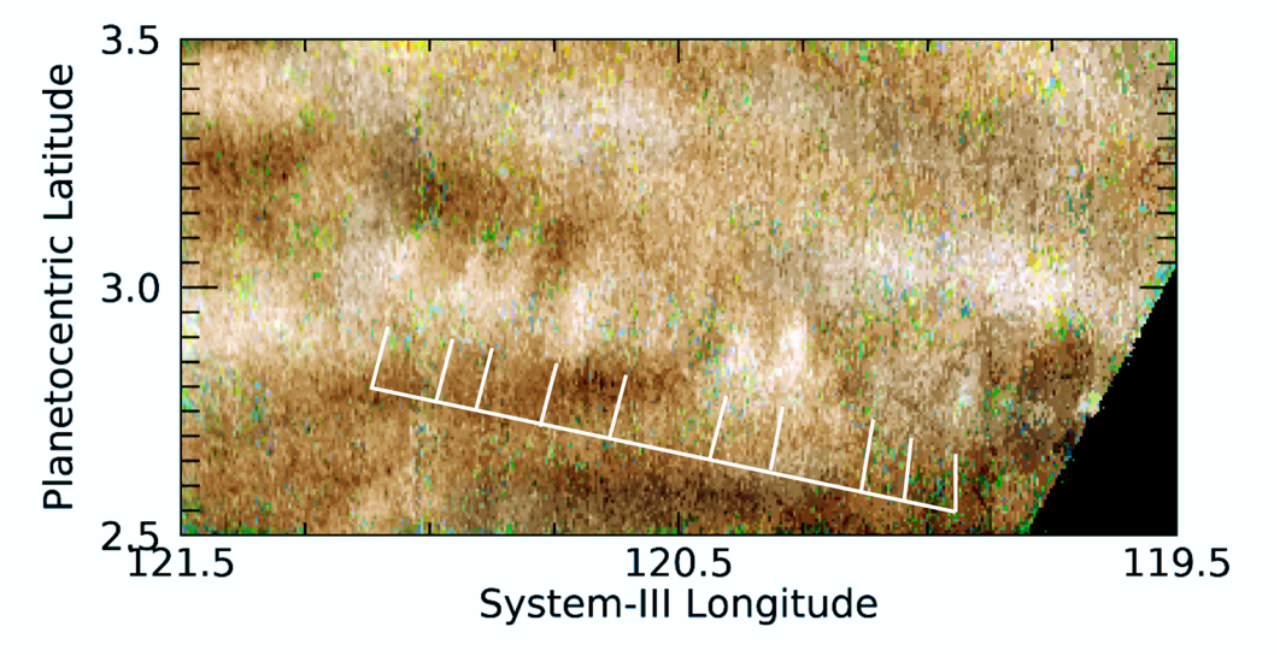

Figure PJ10_30b. JNCE_2017350_10C00030_V01. Some very subtle waves remain detectable in this image after substantial processing to remove green striping artefacts.

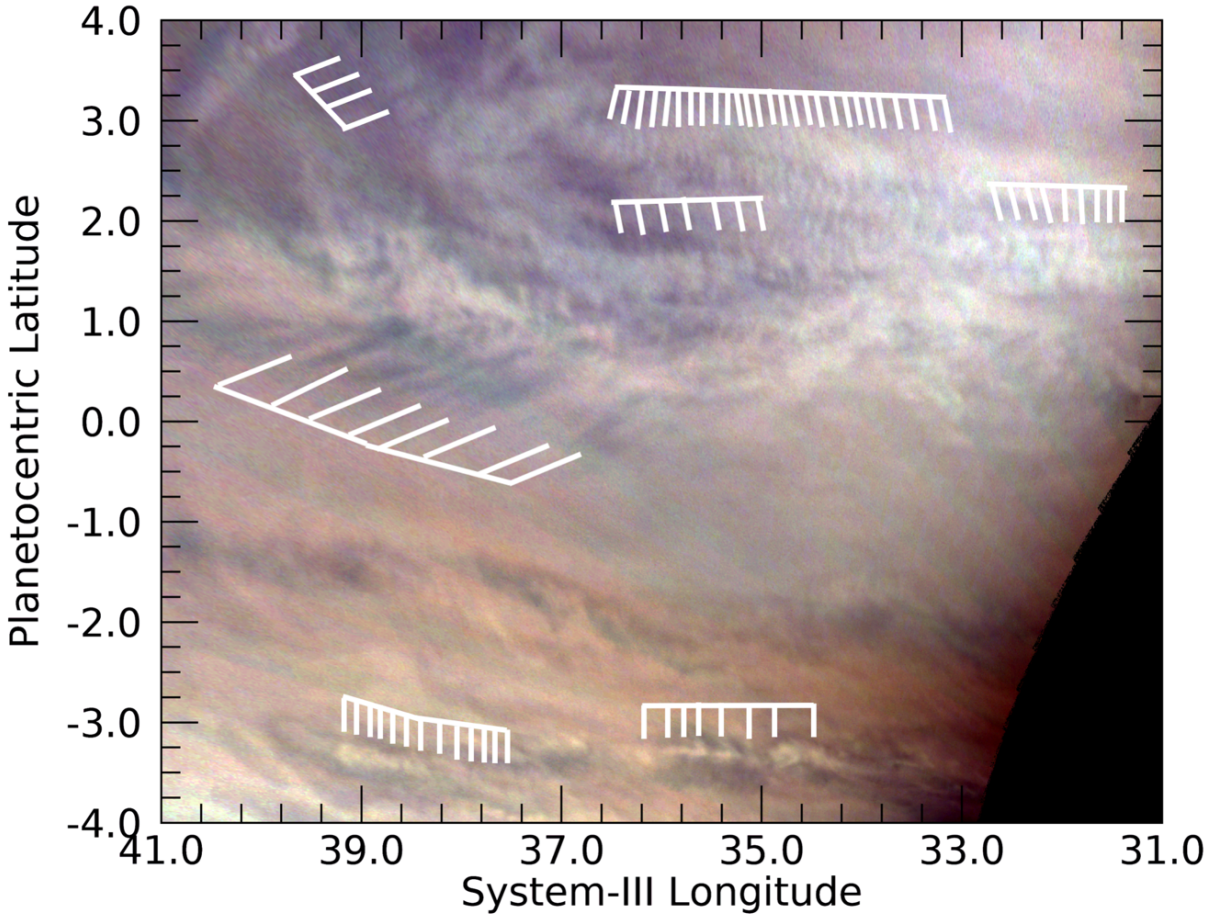

Figure PJ11_20. JNCE_2018038_11C00020_V01. Several waves trains, some of which are overlapping, are evident in this image. We identify several of these by grids of white lines.

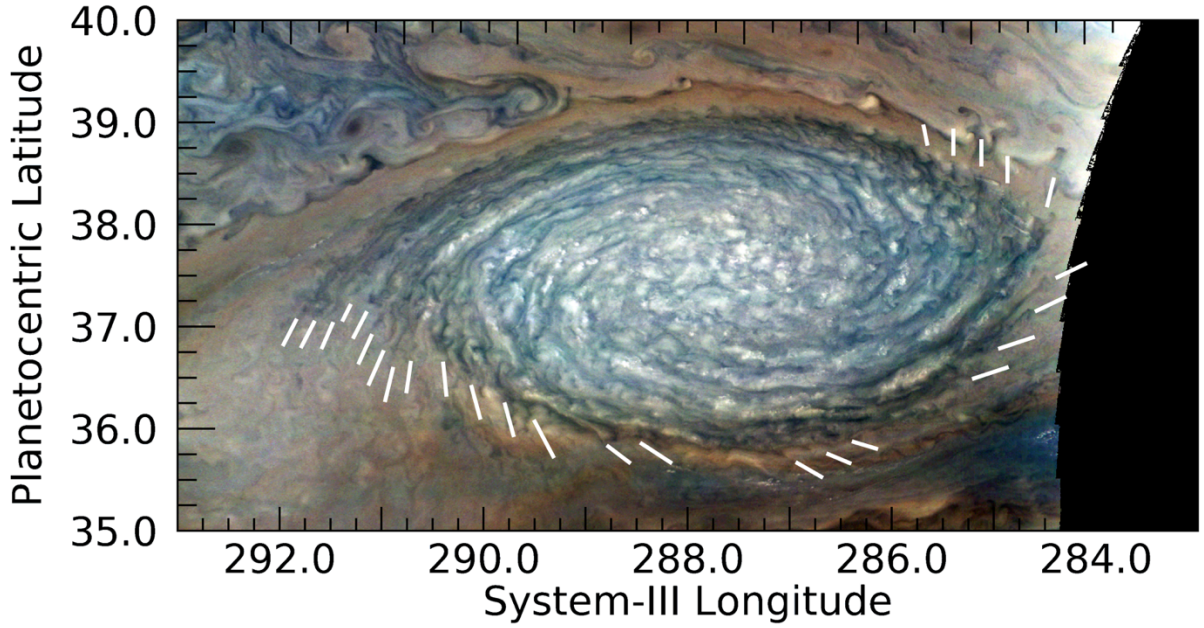

Figure PJ12_85. JNCE_2018001_12C00085_V01. A series of bands can be detected that are associated with the ends of the internal spiral structures within a prominent anticyclonic white oval. Reminiscent of bands of clouds in terrestrial hurricanes, they are more or less regularly spaced. Some individual discrete white clouds can be seen in the ridges that define the spiral structure, but they are insufficiently resolved to determine whether a regular spacing exists between them.

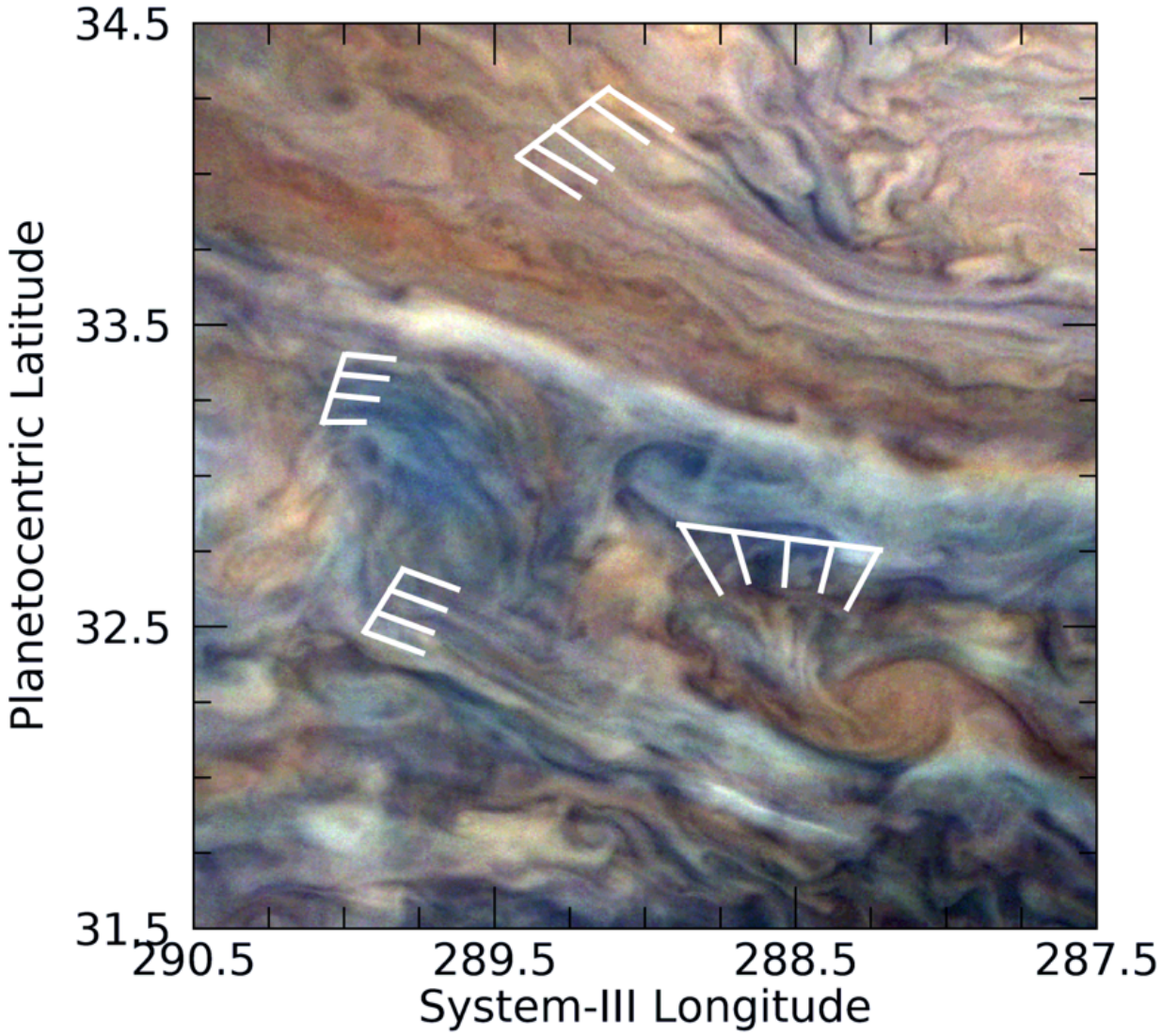

Figure PJ12_86b. JNCE_2018001_12C00086_V01. Multiple examples of aligned cloud streaks with very different orientations are visible in this turbulent part of the North North Temperate Belt. These are similar to those, for example, in Figs. PJ3_109c and PJ5_108, showing that they are common.

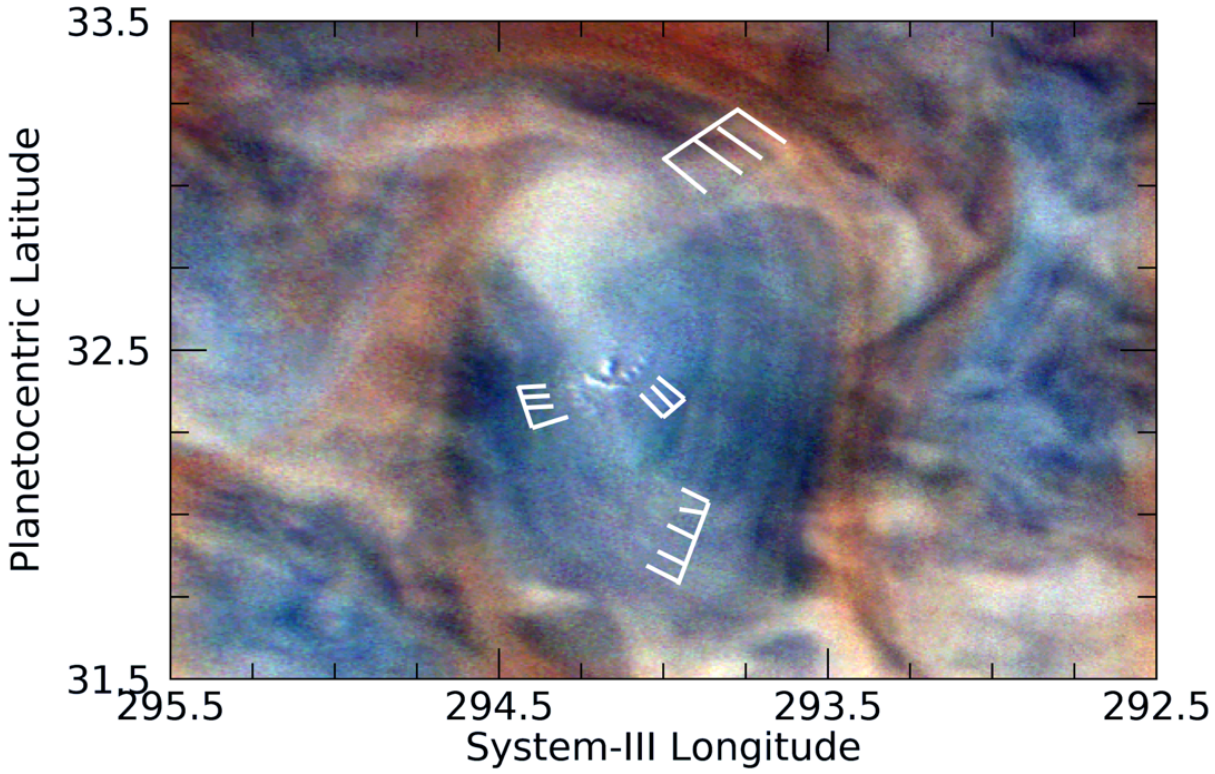

Figure PJ12_86c. JNCE_2018001_12C00086_V01. Close examination of this region, also in the North North Temperate Belt and due west of the area in Fig. PJ12_86a, shows not only cloud streaks but also much finer-scale features. The most unexpected were the few small, bright clouds, all of which subtend shadows and extend higher than the surrounding darker region. Verifying that they are not an artefact in the imaging, we note that they are present – although at lower resolution – in the image taken prior to this one (JNCE_2018001_12C00085_V01).

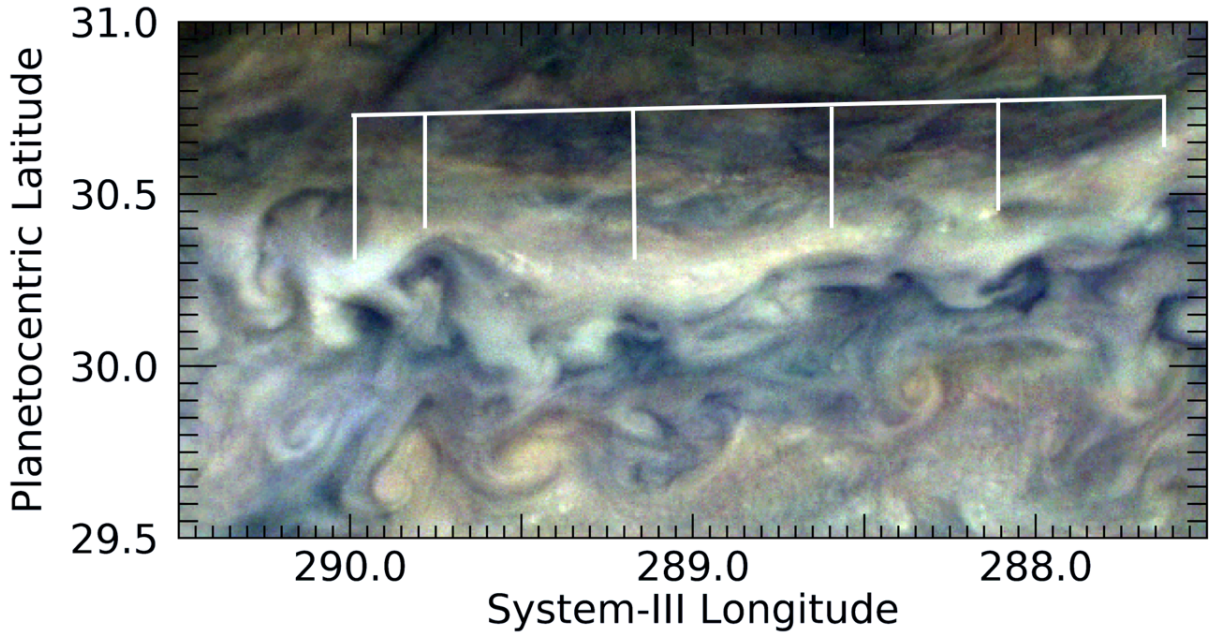

Figure PJ12_86d. JNCE_2018091_12C00086_V01. Prominent repeated patters are seen along the southern edge of an unusual white band located at the turbulent boundary between the northern and southern components of the North Temperate Zone. It is not clear that these can be classified as waves.

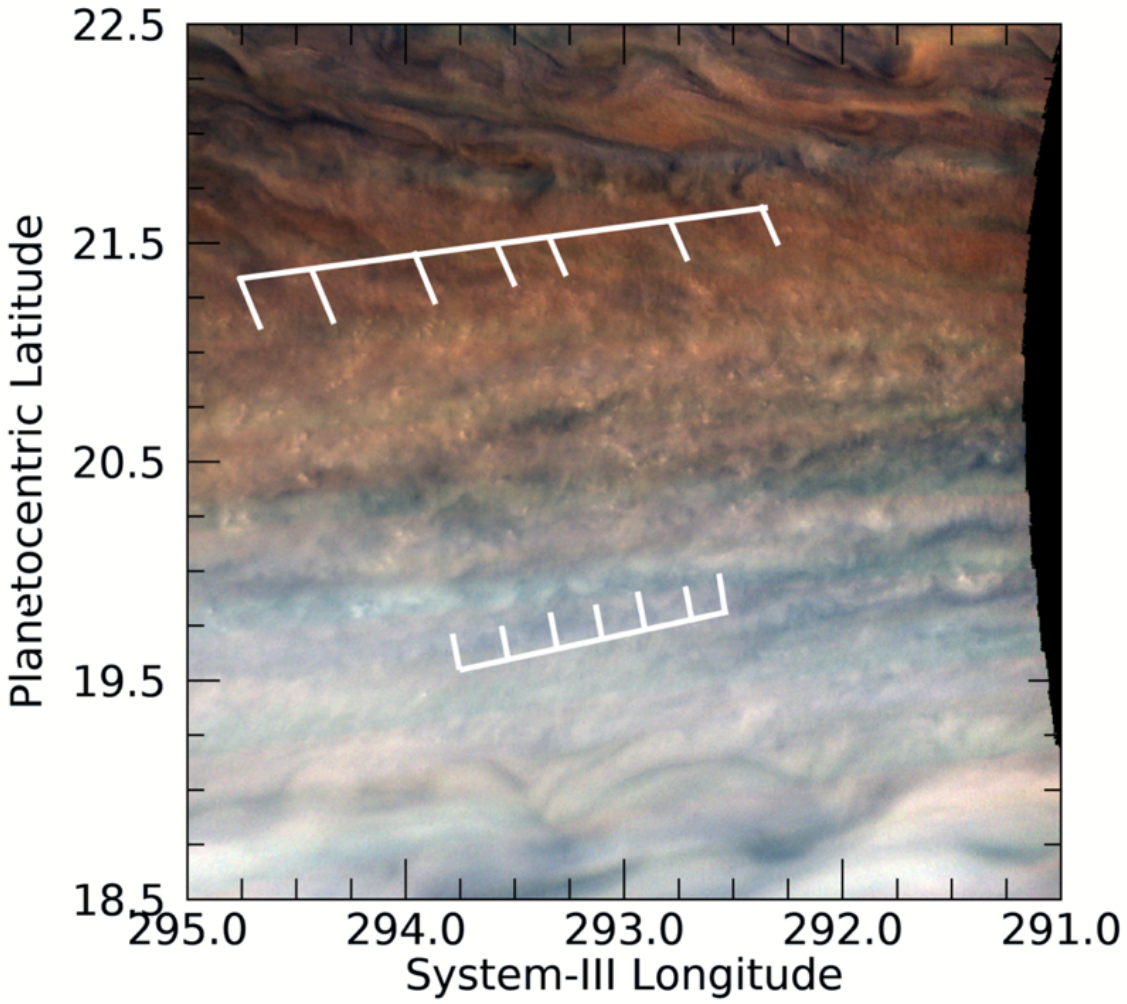

Figure PJ12_87b. JNCE_2018091_12C00087_V01. Repeated wave-like features (lower grid) and regular clusters of clouds (upper grid) are detectable in this image. The latter probably represent a pattern that barely meets our criterion for consideration as a wave-like feature.

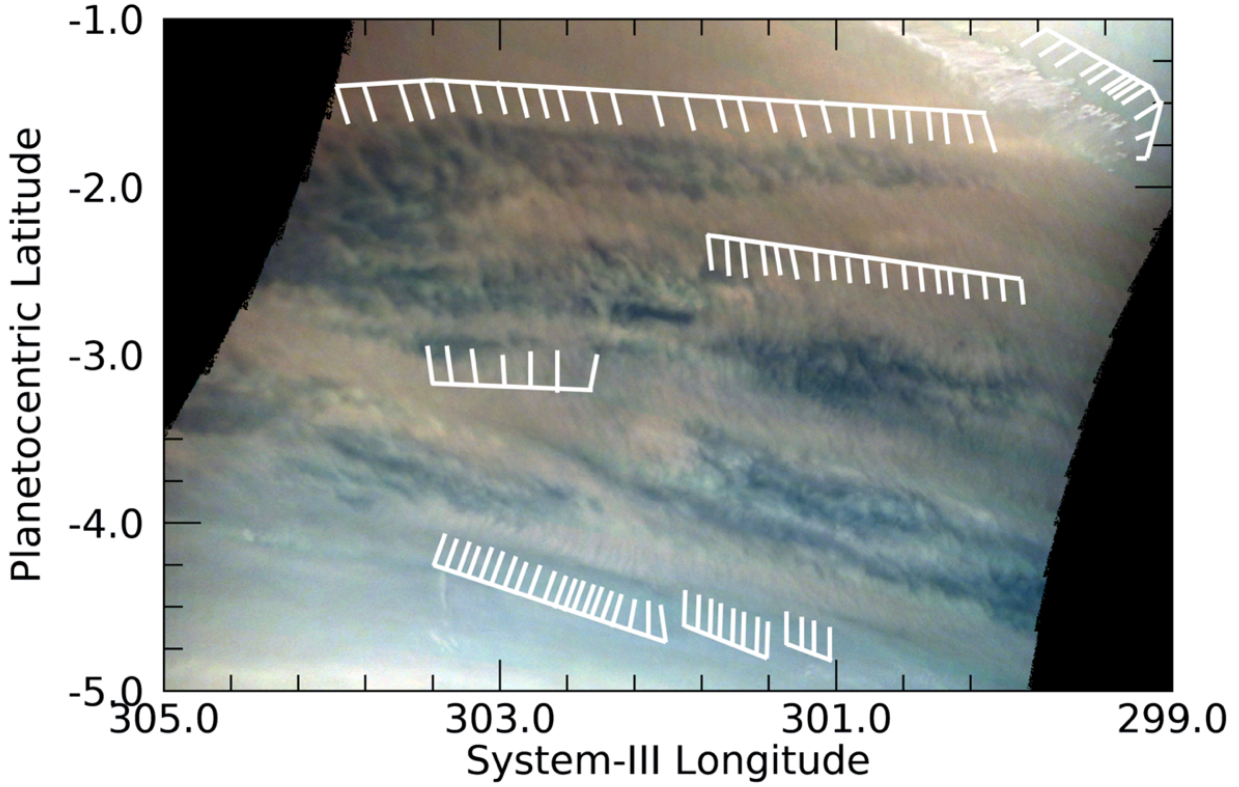

Figure PJ12_90a. JNCE_2018091_12C00090_V01. Several packets of waves are detectable at all latitudes in this image; we indicate several of them by the grids of white lines. This is the first PJ at which images of the Equatorial Zone were returned at maximum quality specifically for the purpose of examining these waves.

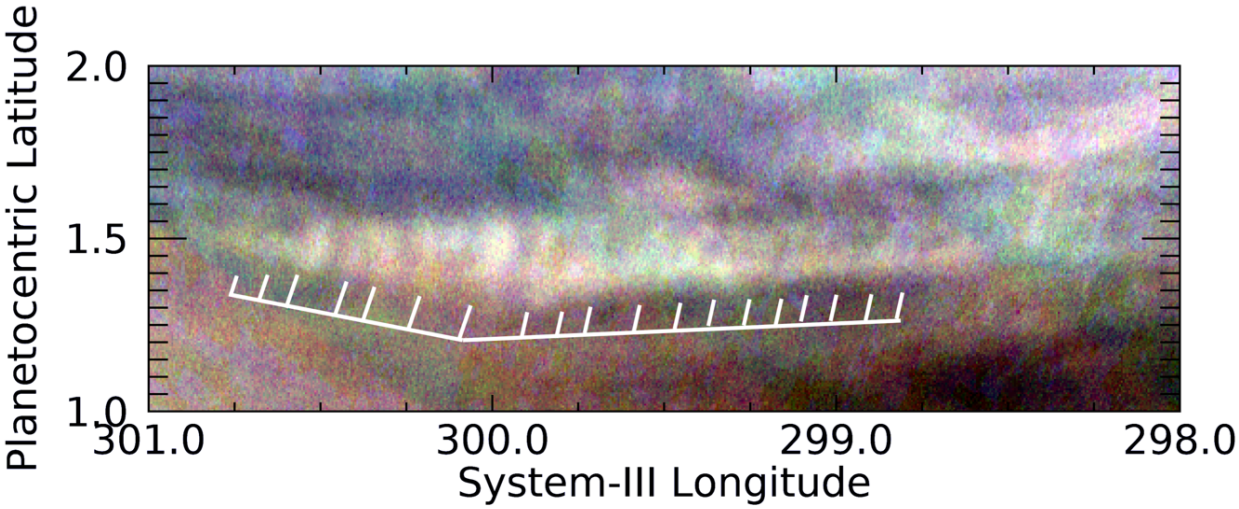

Figure PJ12_90b. JNCE_2018091_12C00090_V01. A pattern of waves associated with a relatively brighter cloud pattern in the Equatorial Zone is evident above the noise of this image.

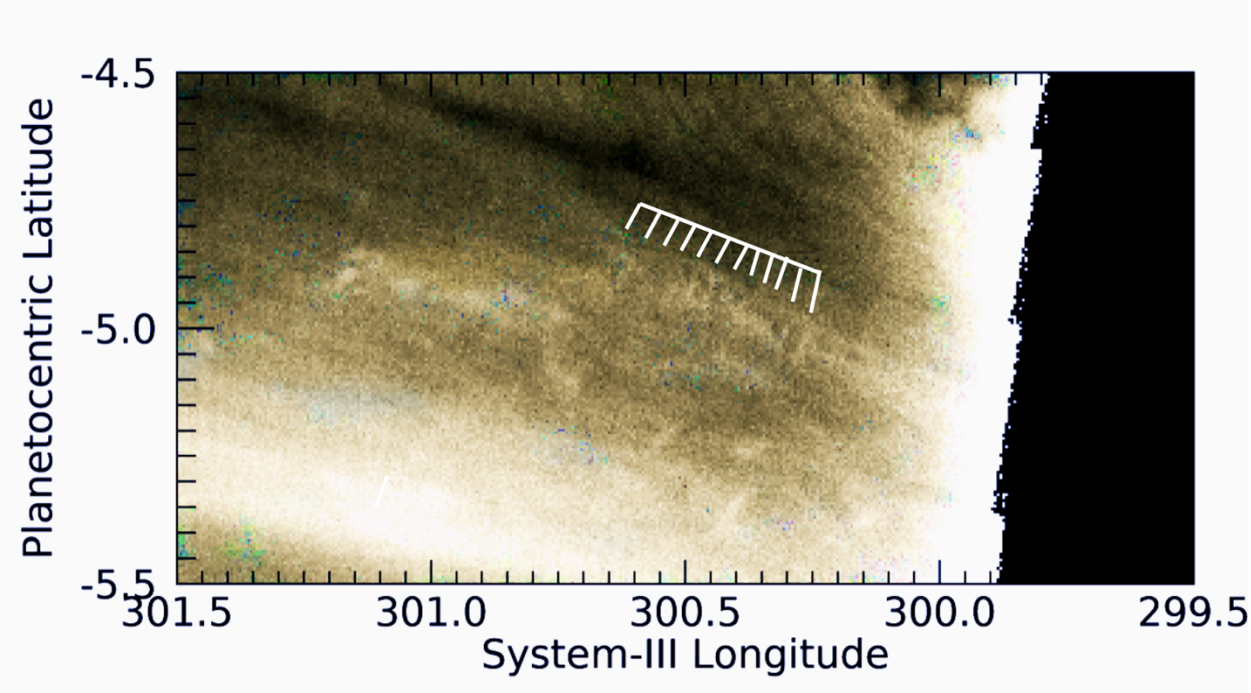

Figure PJ12_90c. JNCE_2018091_12C00090_V01. These very subtle wave-fronts in the Equatorial Zone are detectable above the noise in all three filters. Color-adjustment processing has been done to remove striped artefacts from the image.

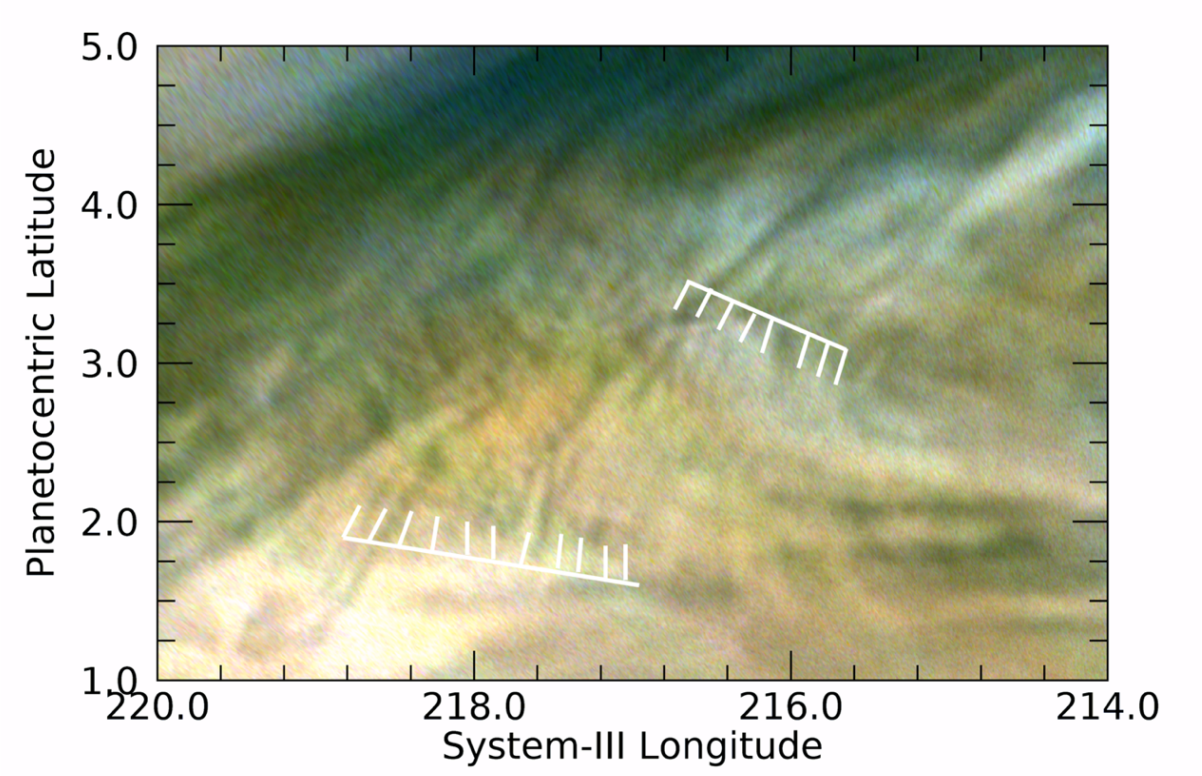

Figure PJ13_35a. JNCE_2018144_13C00035_V01. A series of elongated waves in the Equatorial Zone is detected in this image.

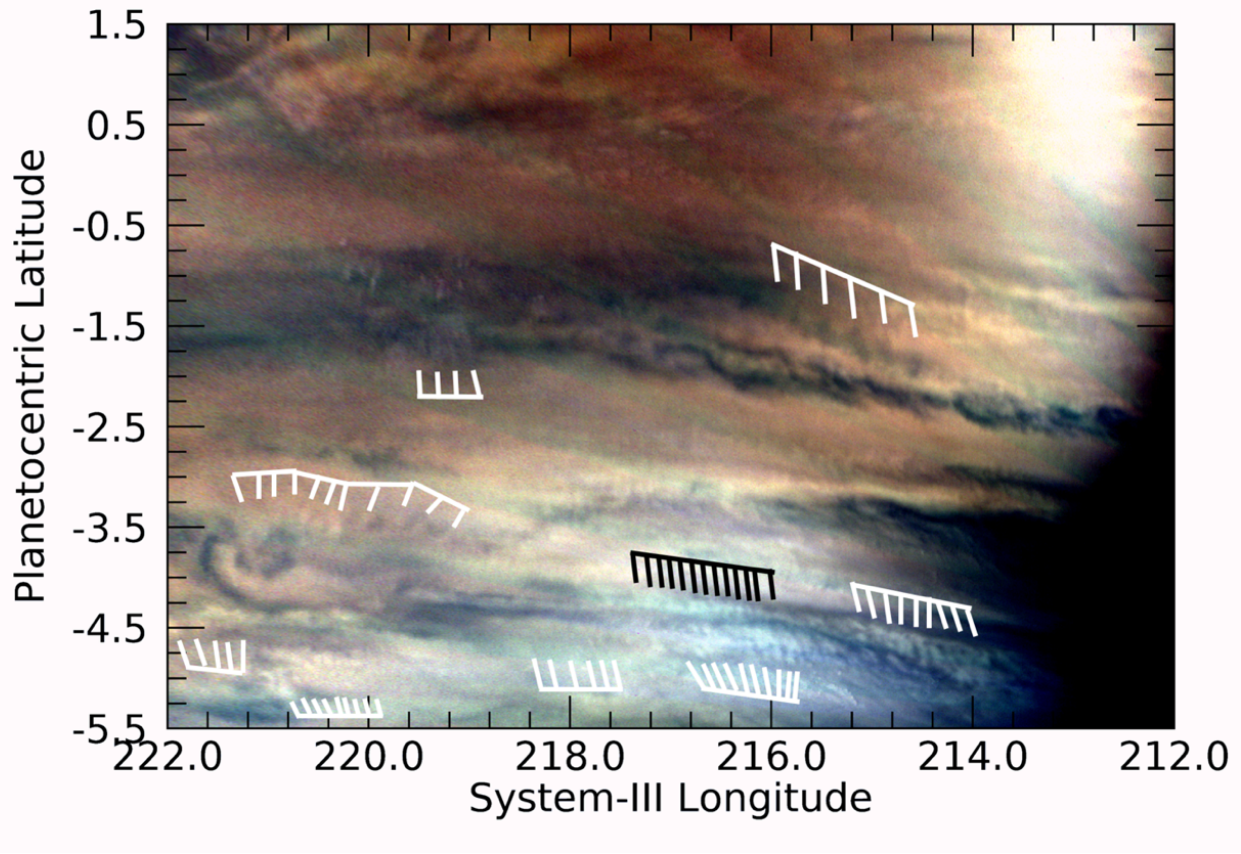

Figure PJ13_35b. JNCE_2018144_13C00035_V01. Many wave packets are detectable in and along the southern edges of the Equatorial Zone and into the South Equatorial Belt. Several of these are indicated in this figure.

.

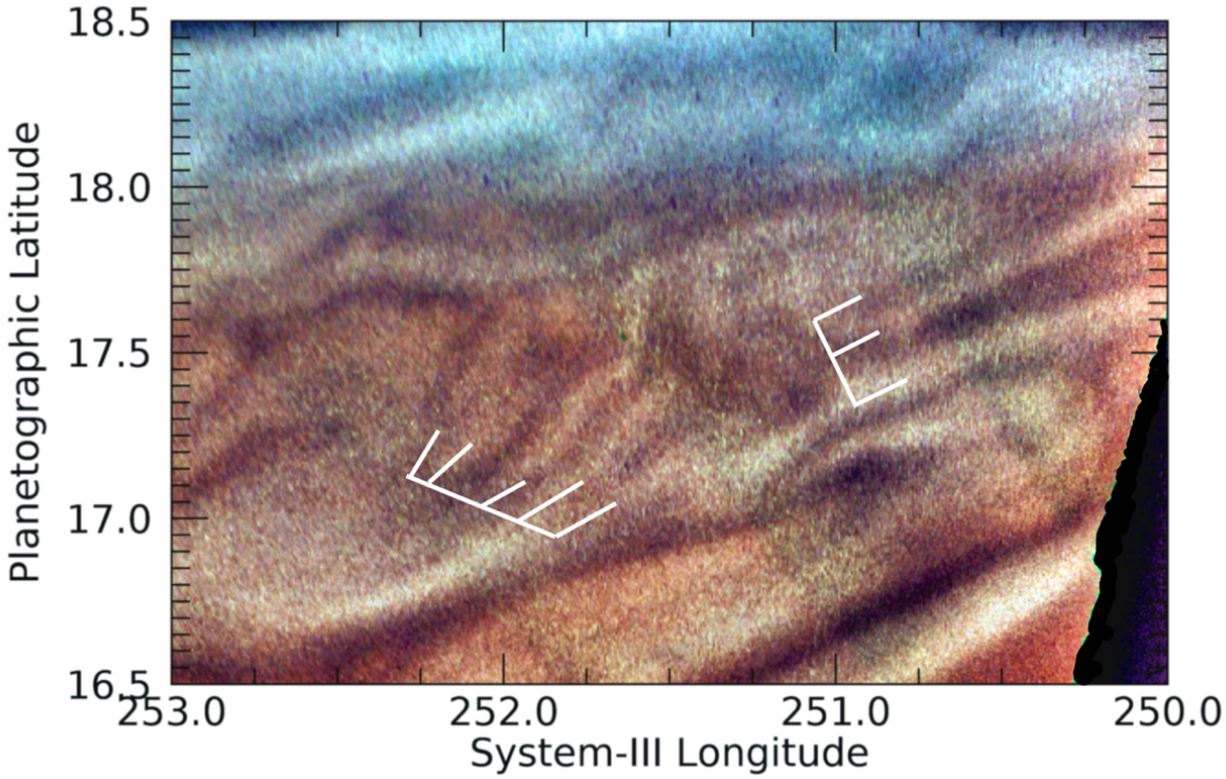

Figure PJ14_25a. JNCE_2018197_14C00025_V01. These dark streaks are in a yellowish strip of the North Tropical Zone, just north of the NEBn retrograde jet where it flows around a barge, a part of which is seen in the bottom-right-hand corner of this figure. The most prominent streaks in the lower part of the figure may be aligned with the jet and represent flow lines.

(Note that we were most successful in minimizing the artificial green stripes in this image by combining the regular map and a high-passed version of the map, decomposing both into three HSL - hue, saturation, lightness - channels and combining the L component of the high-passed map, with the H and S components of the regular map to create a colorized map of high contrast.)

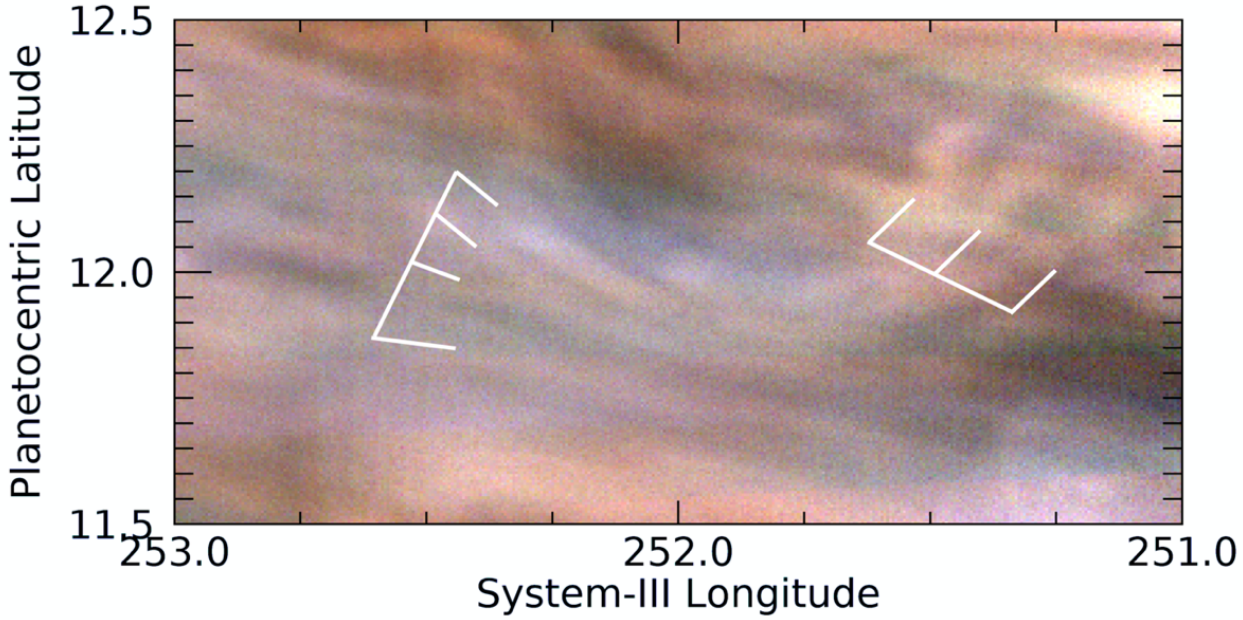

Figure PJ14_25b. JNCE_2018197_14C00025_V01. Repeated patterns are detectable in these otherwise diffuse streaks in the North Equatorial Belt.

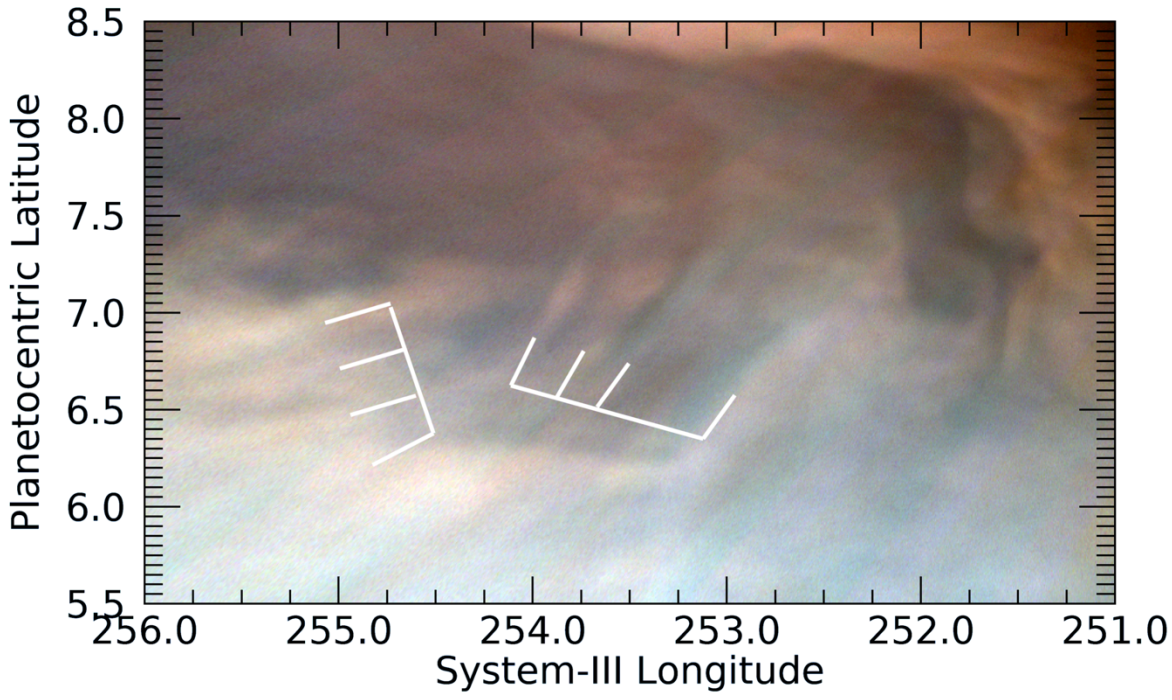

Figure PJ14_25c. JNCE_2018197_14C00025_V01. Similar to the features in Fig. PJ14_25b, Repeated wave-like patterns are detectable here at the boundary between the Equatorial Zone and the North Equatorial Belt. (For both this and the previous figure, the color stretch was softened in order to minize the appearance of artefactual colored stripes.)

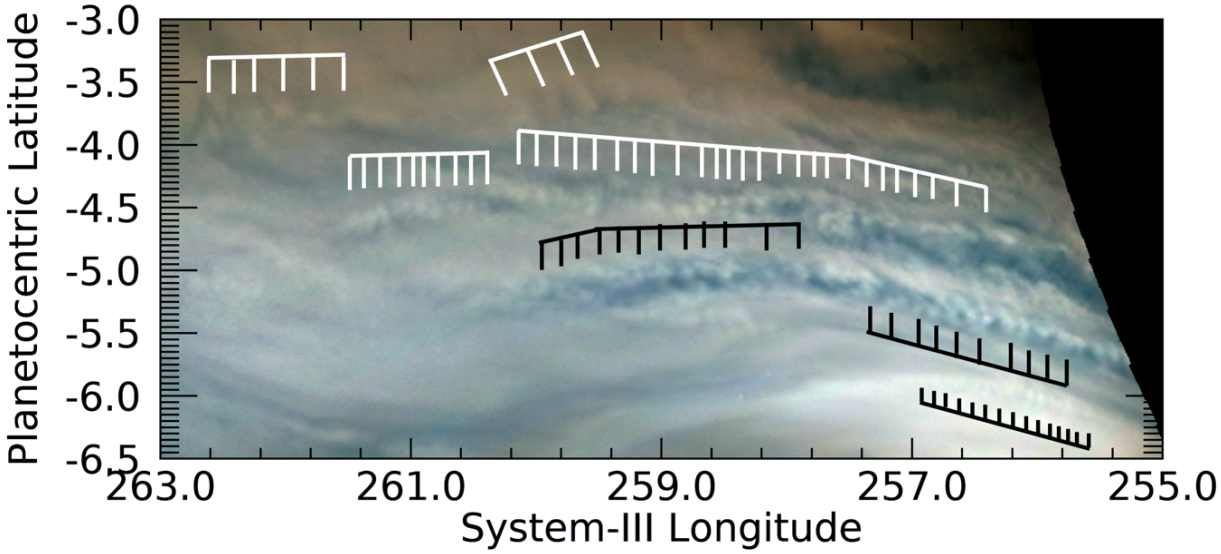

Figure PJ14_28a JNCE_2018197_14C00028_V01. Multiple wave packets are observable in this region of the Equatorial Zone.

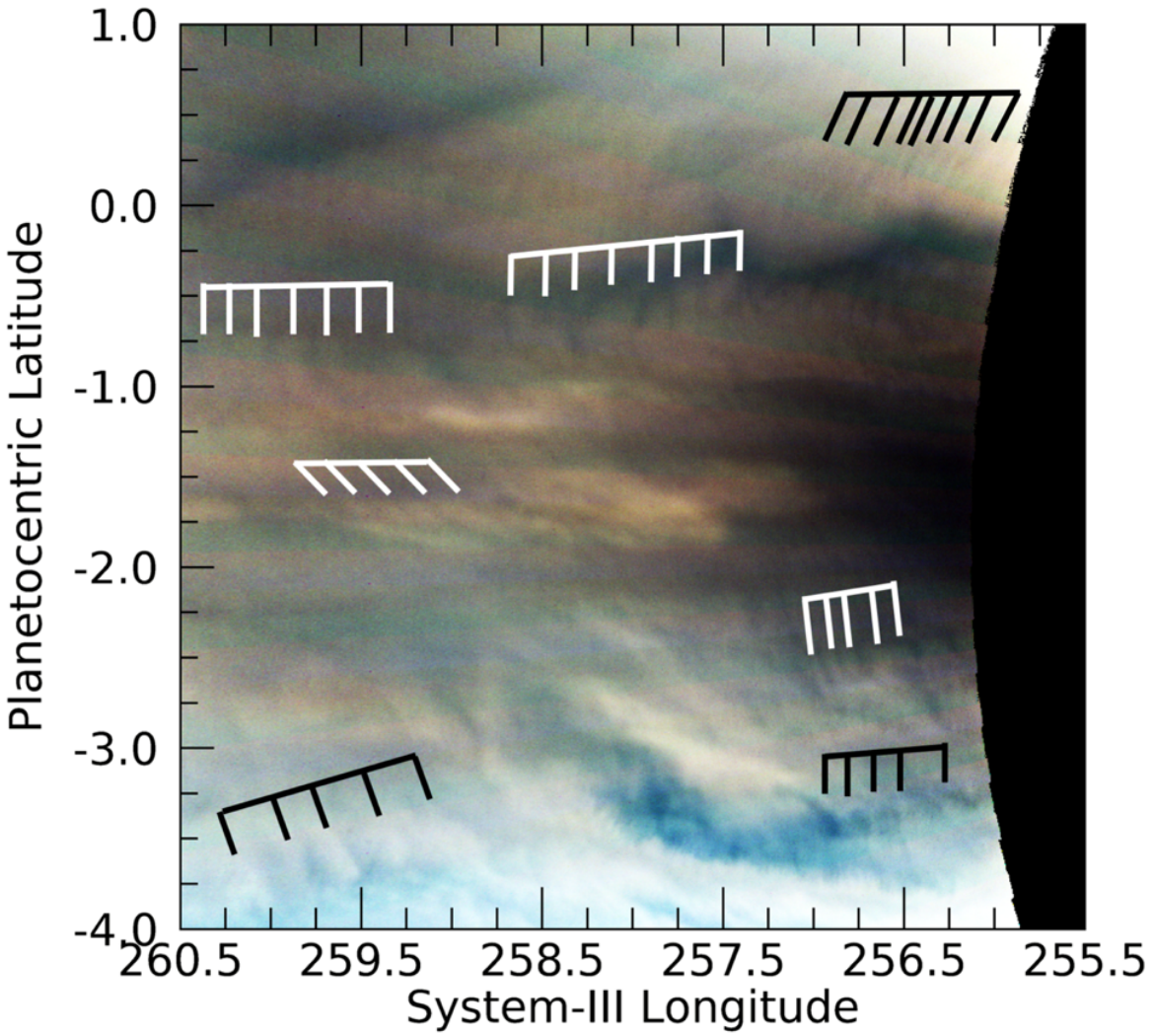

Figure PJ14_28b. JNCE201819714C00028V01. Several wave packets can be detected in this image of the Equatorial Zone, which overlaps slightly with Figure PJ14_28a.

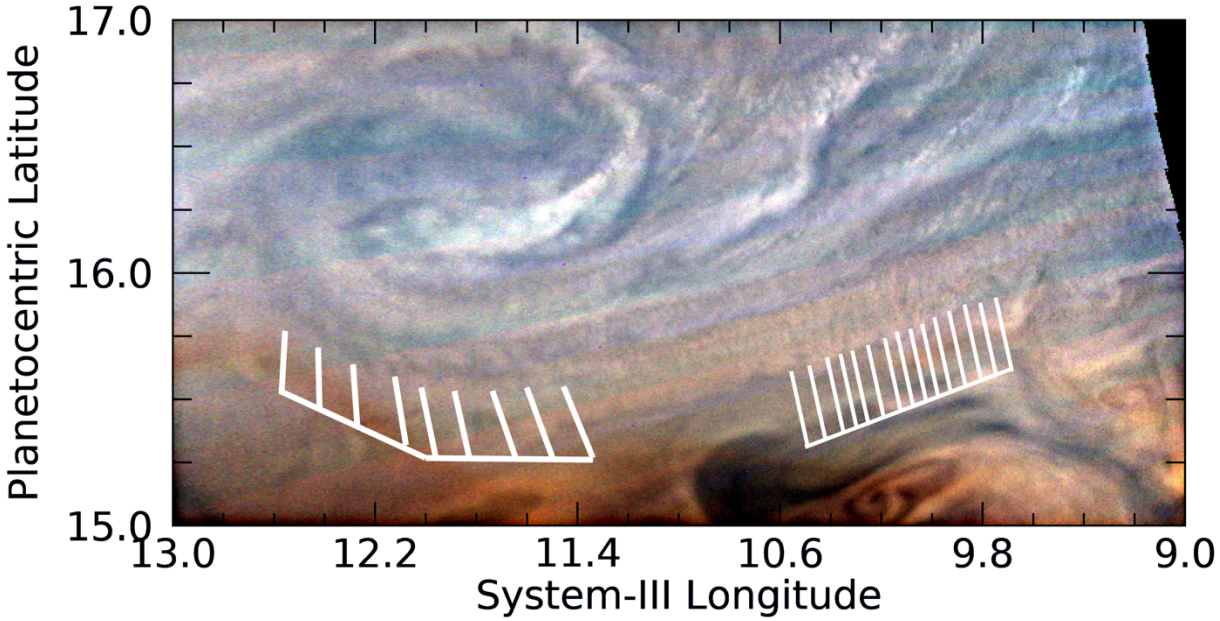

Figure PJ15_26. JNCE_2018250_15C00026_V01. Wave packets with different size wavelengths can be resolved in this region immediately south of a anticyclonic eddy in the northern component of the North Equatorial Belt (NEBn).

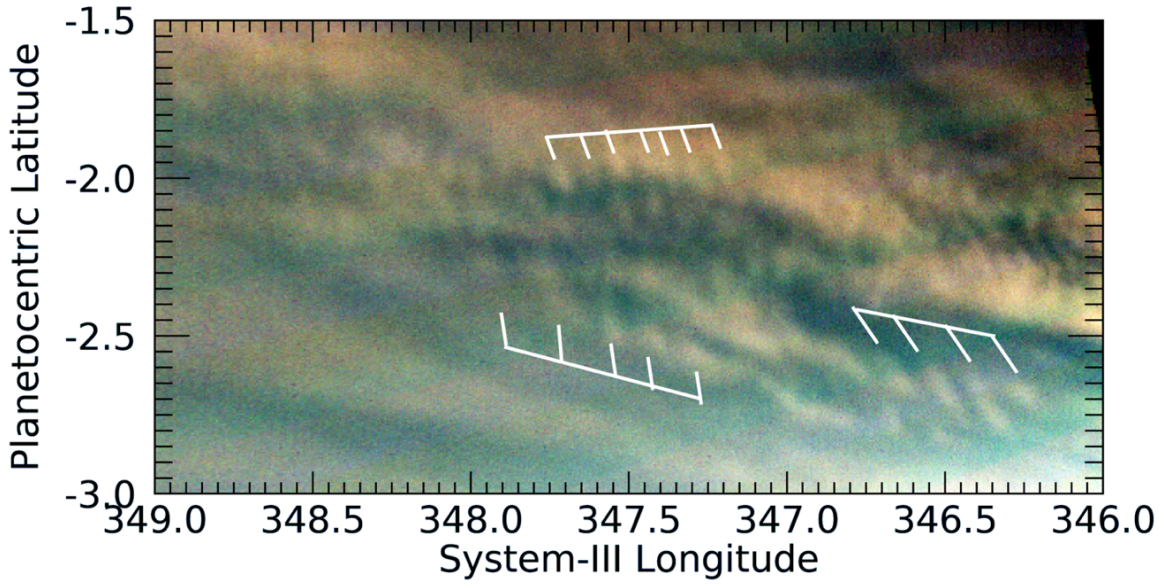

Figure PJ15_29. JNCE_2018250_15C00029_V01. Several wave packets are present in this image, three of which are indicated by the white grids.

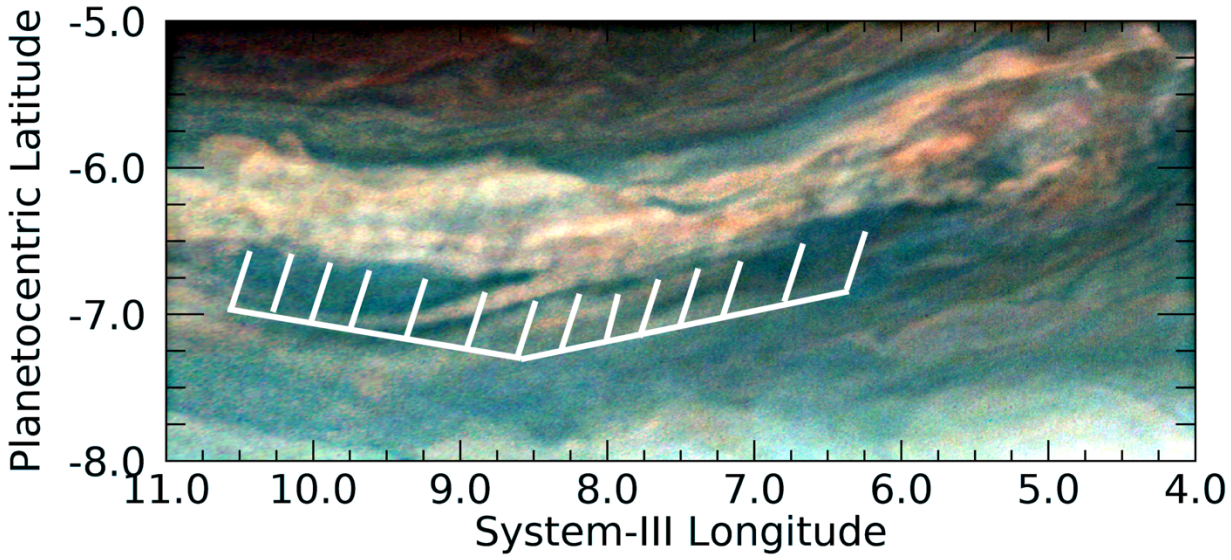

Figure PJ15_31. JNCE_2018250_15C00031_V01. Several waves are seen in this packet that are associated with a white region on the southern edge of a dark cyclonic vortex, known as a "barge" in the South Equatorial Belt. Some unsharp masking has been applied to this image in order to make the faint waves more prominent.

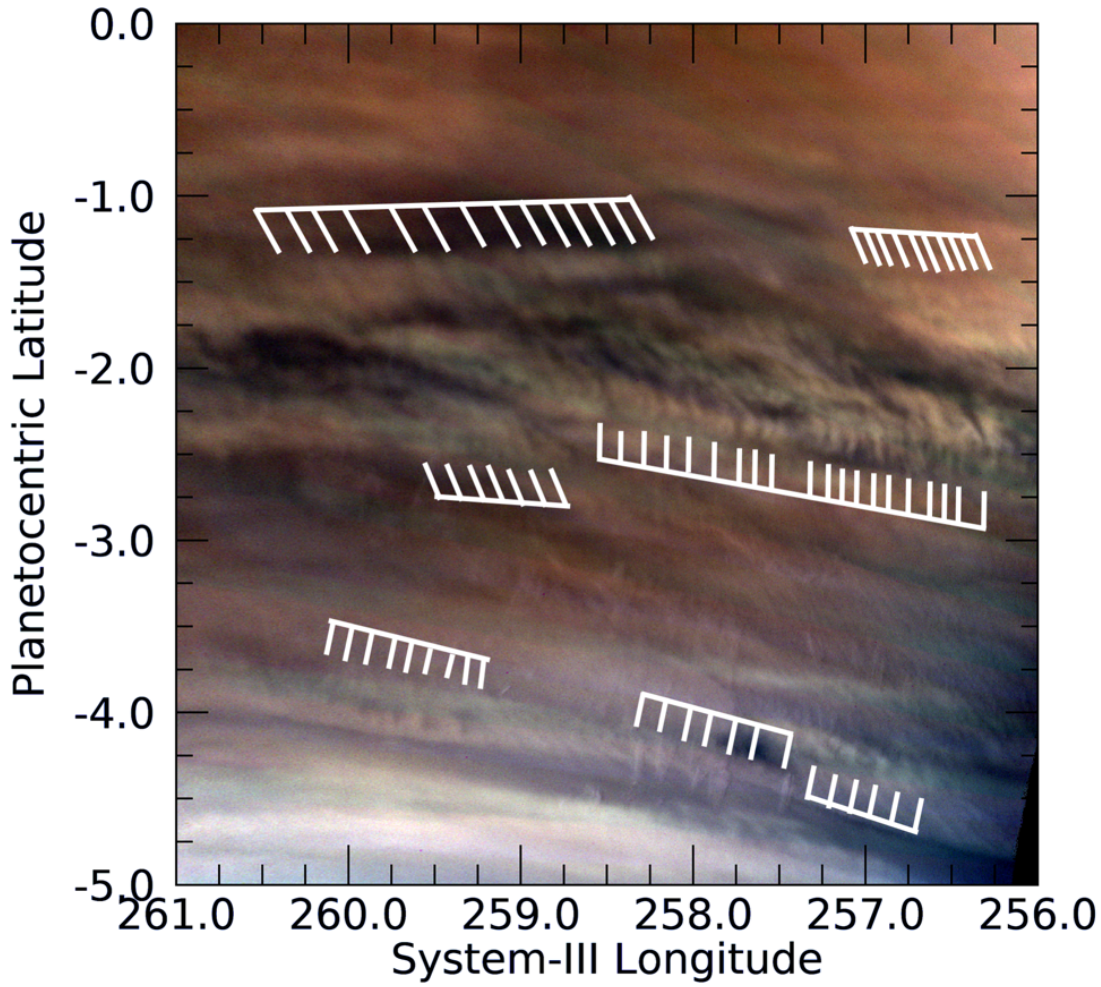

Figure PJ16_20. JNCE_2018302_16C00020_V01. Multiple wave packets are detectable in this image of the Equatorial Zone, several of which are indicated by the white grid lines. Many wavefronts are nearly perpendicular to the direction of the wave packet.

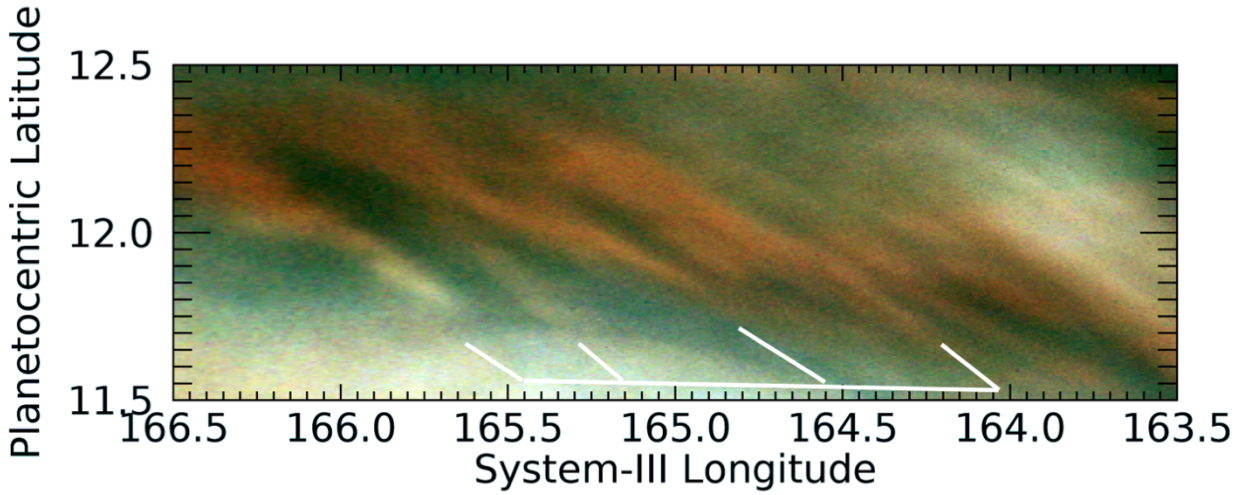

Figure PJ17_24. JNCE_2018355_17C00024_V01. Some streak-like features are detected in the middle of the North Equatorial Belt. This region is dominated by cyclonic motion, so the organization of this feature parallels the zonal-wind gradient. The exaggerated large-scale diffuse color contrast across the image may represent diffuse bands of white or reddish haze overlying the main cloud deck.

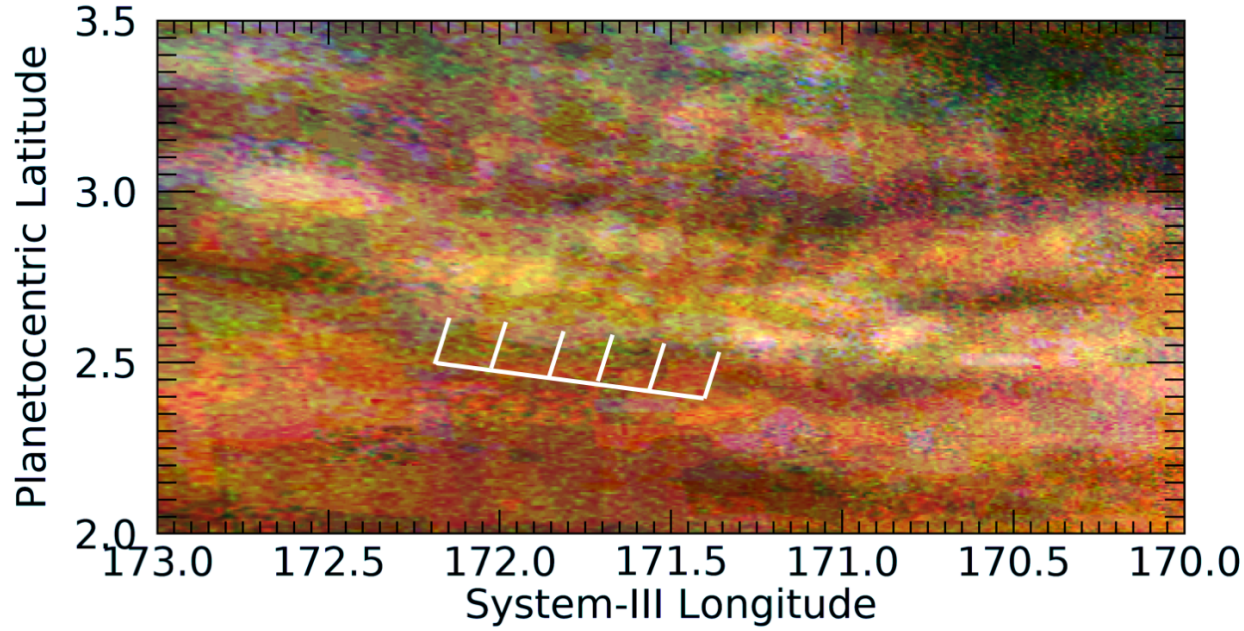

Figure PJ17_26. JNCE_2018355_17C00026_V01. A short, relatively faint wave packet is detectable in this image of the Equatorial Zone.

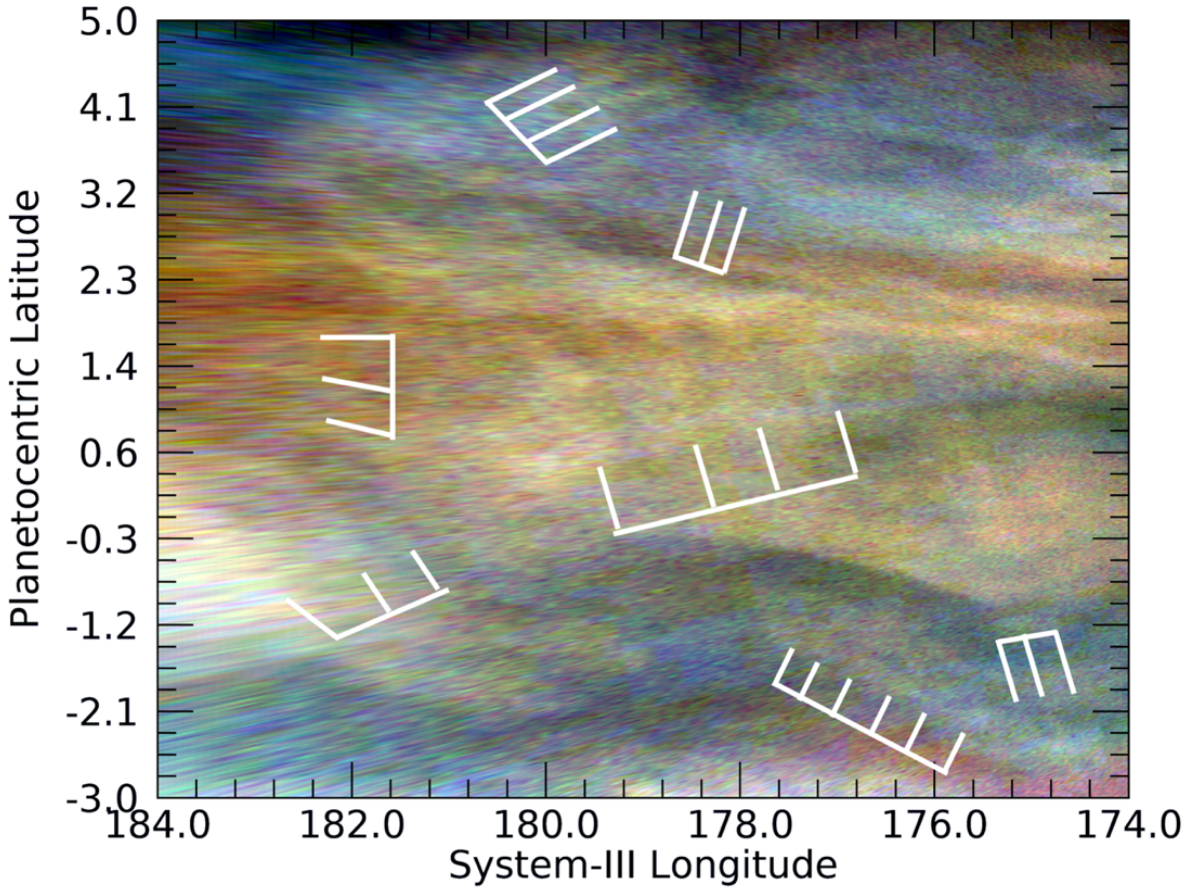

Figure PJ17_24a. JNCE_2018355_17C00024_V06. Several wave packets, some overlapping, are detectable in this image of the Equatorial Zone, with several indicated by the white grids.

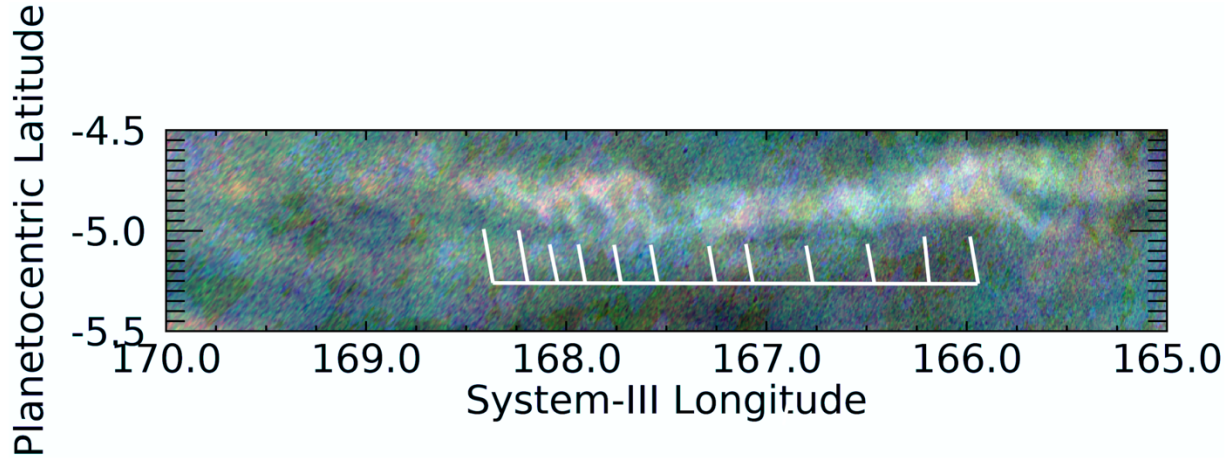

Figure PJ17_24b. JNCE_2018355_17C00024_V06. A short sequence of discrete features is evident in this image of a region within the Equatorial Zone.

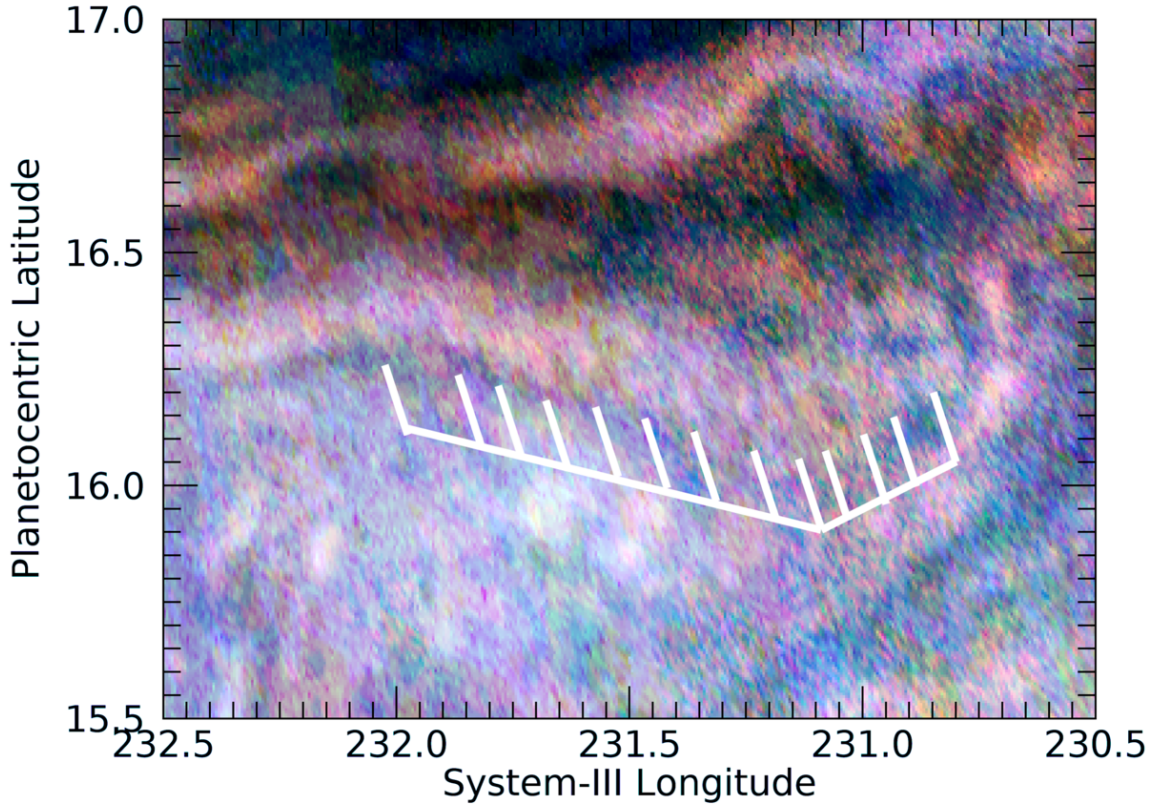

Figure PJ18_34. JNCE_2019043_18C00034_V01. Very faint waves are detectable above the noise in this image. (Note that the extreme stretching needed to display the waves is responsible for the unusual color scheme of this figure.)

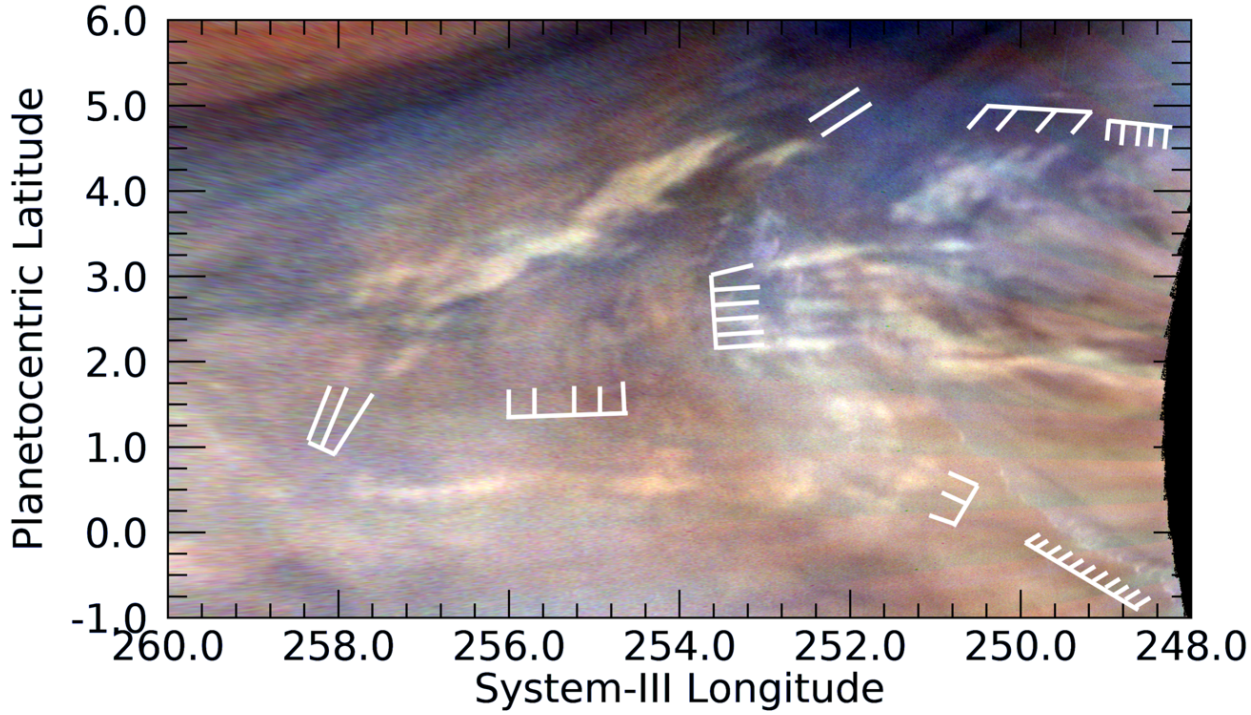

Figure PJ18_38. JNCE_2019043_18C00038_V01. This region in the northern component of the Equatorial Zone is filled with overlapping waves, several of which are indicated by the white grid lines.

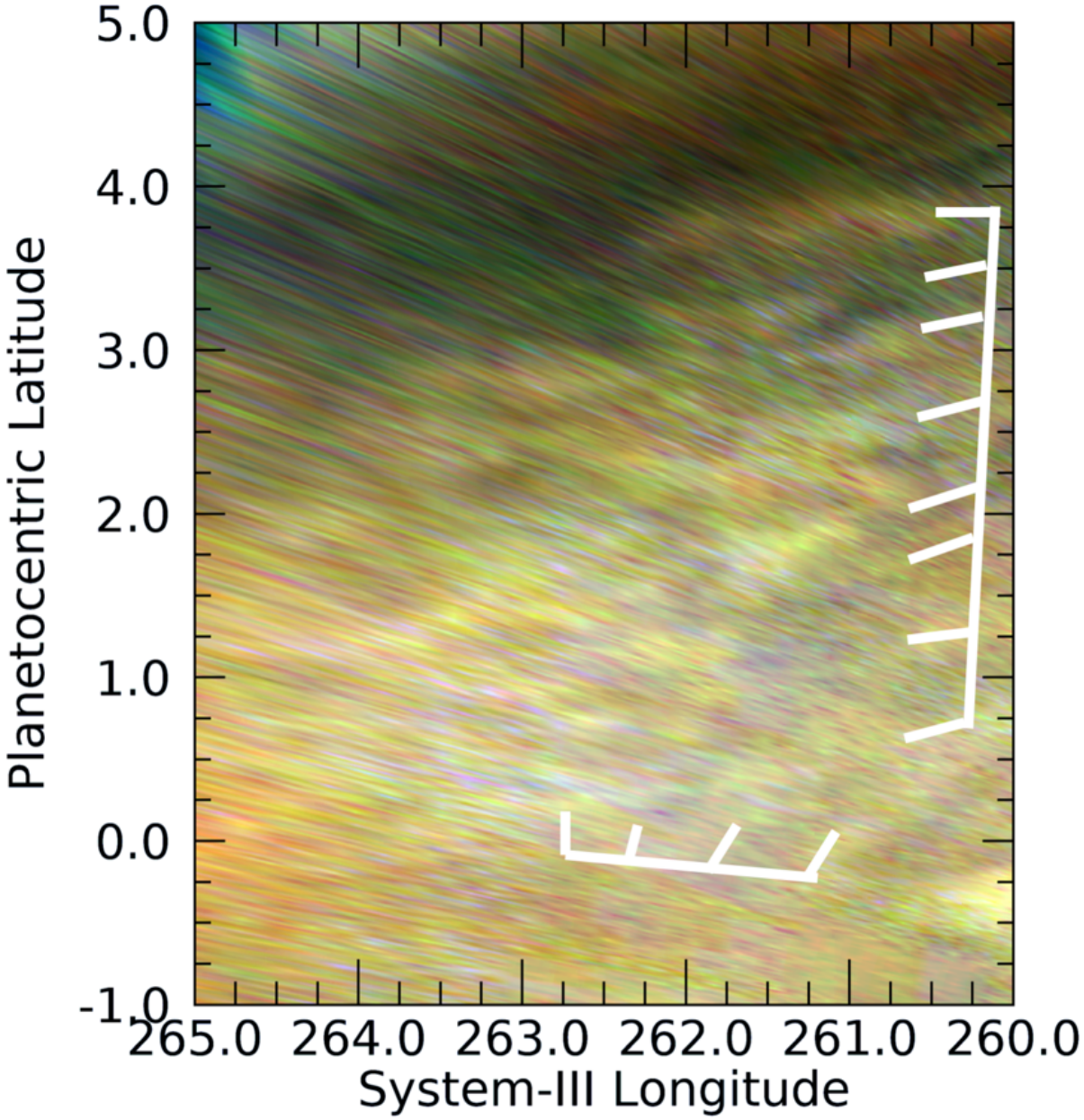

Figure PJ18_39a. JNCE_2019043_18C00039_V01. Several independent wavefronts are detectable in cross directions are detectable in this image of the Equatorial Zone, two of which are indicated by the white grids. This region is immediately to the west of the region shown in Figure PJ18_39b.

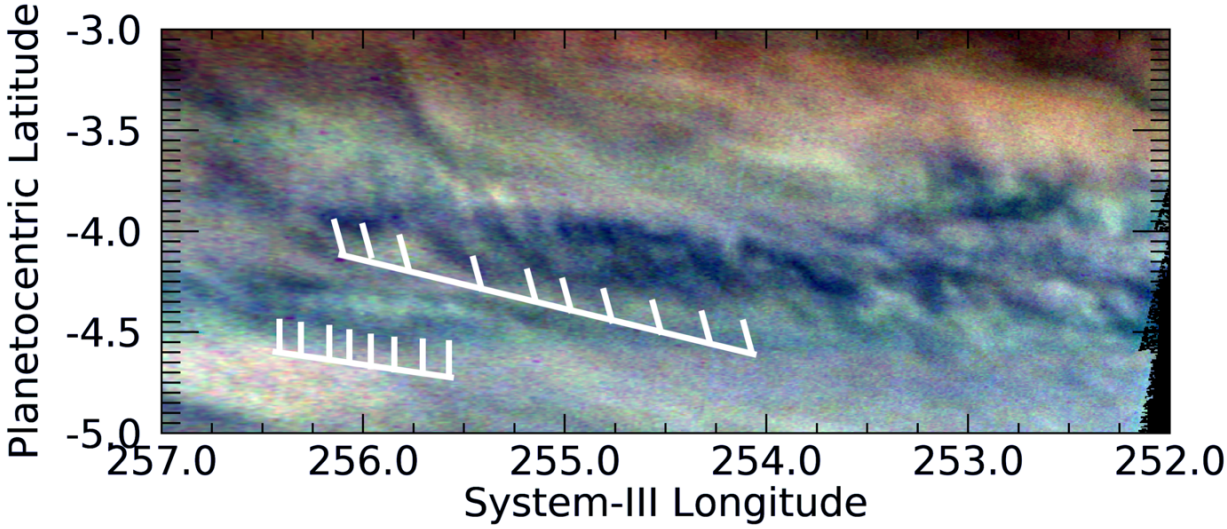

Figure PJ18_39b. JNCE_2019043_18C00039_V01. Very faint waves are detectable in this image of the southern component of the Equatorial Zone.

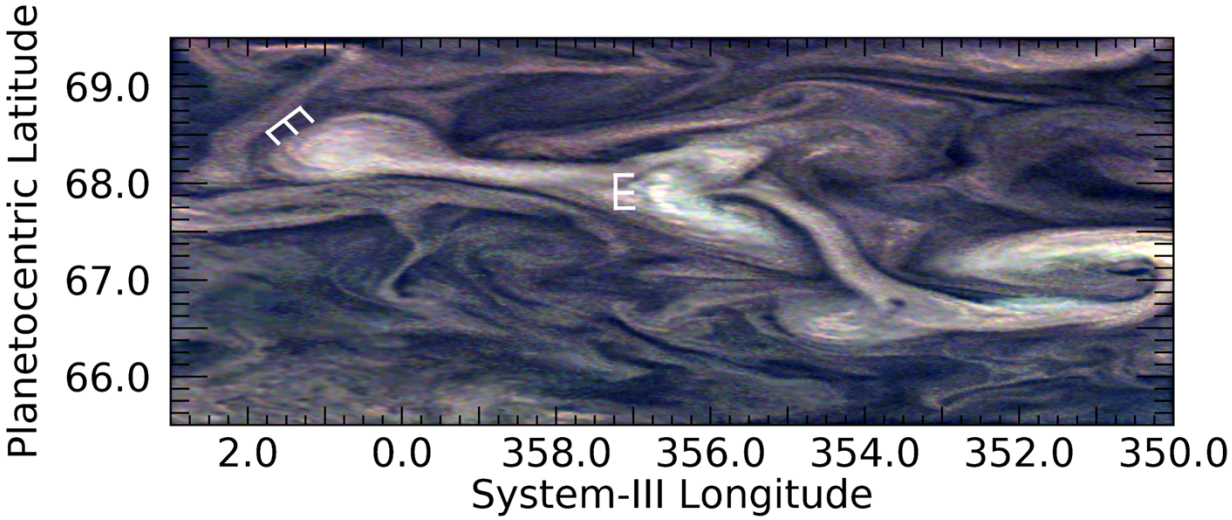

Figure PJ20_24 JNCE_2019043_20C00024_V01. A regular sequence of three bright cloud features can be seen within a branch of a relatively bright feature with two distorted lobes to the east and west of the features indicated by the white grid. The white grid in the upper left indicates another set of three somewhat offset whitish discrete clouds, just within the resolution of JunoCam. This area is well into the north polar region that is not dominated by zonal winds. It is the furthest north that JunoCam has detected anything resembling a repeatable feature. Moderate unsharp masking has been performed in order to make the subtle features indicated in the upper left more recognizable.

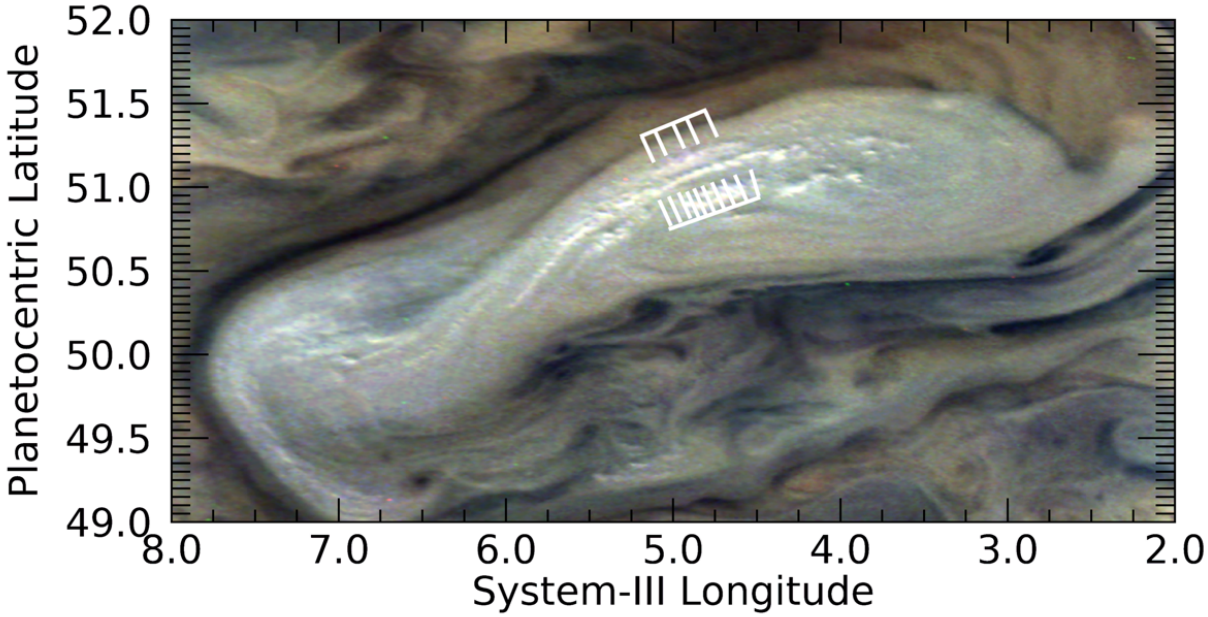

Figure PJ20_26a. JNCE_2019043_20C00026_V01. Regular sequences of variable cloud features can be detected along these cloud banks that are just within the resolution of JunoCam inside this anticyclonic vortex. This region and the one shown in Fig. PJ20_26b are immediately south of the prograde jet at a planetocentric latitude of 53°N.

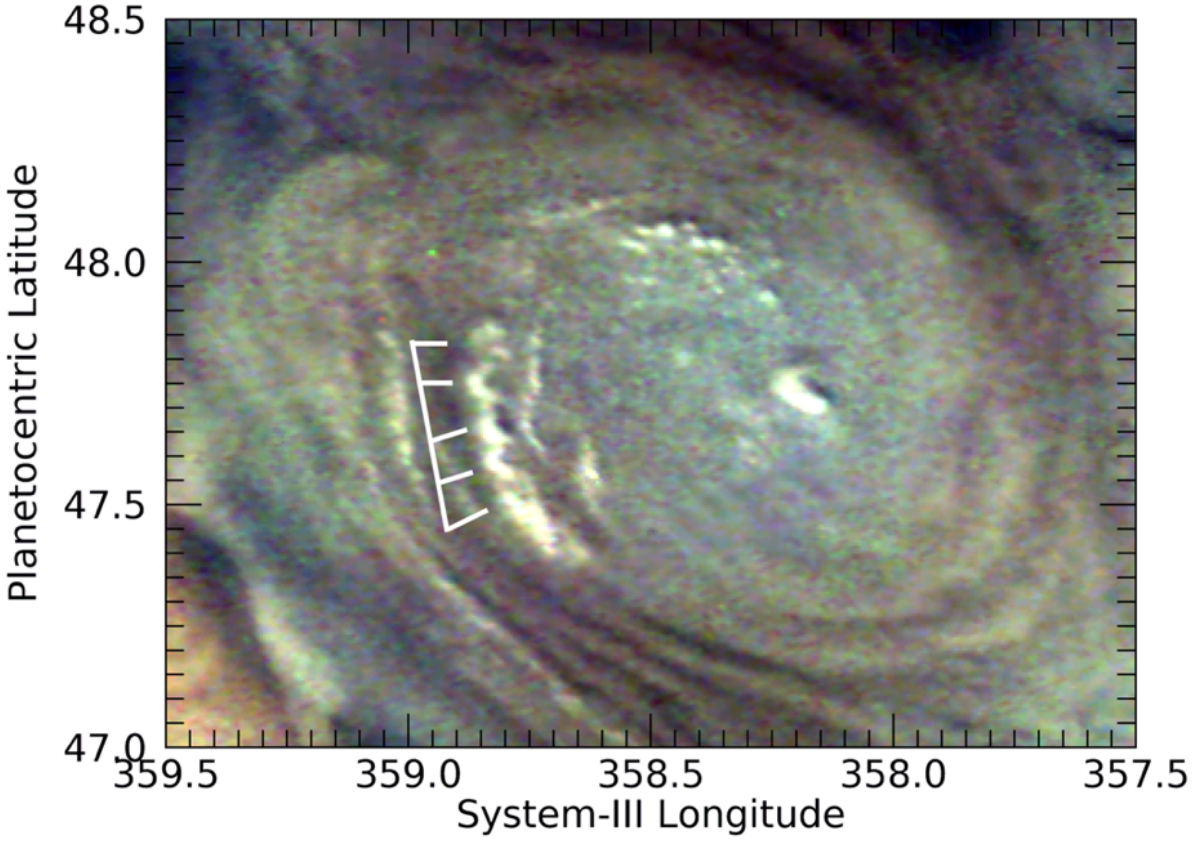

Figure PJ20_26b. JNCE_2019043_20C00026_V01. As in Figure PJ20_1, we detect a regular sequence of variable, somewhat arcuate, cloud features along a curved cloud bank in the western side of this anticyclonic vortex. Banks of clouds such as these and those in Fig. PJ20_26a have been seen in previous perijoves, starting prominently in PJ6, but the regions shown in Figs. PJ04_103b, PJ12_86c, and PJ20_26a and this figure are the only ones in which we have been able to resolve individual cloud components. Thus, they are the only ones in which we have been able to classify them as being a wave-like phenomenon.

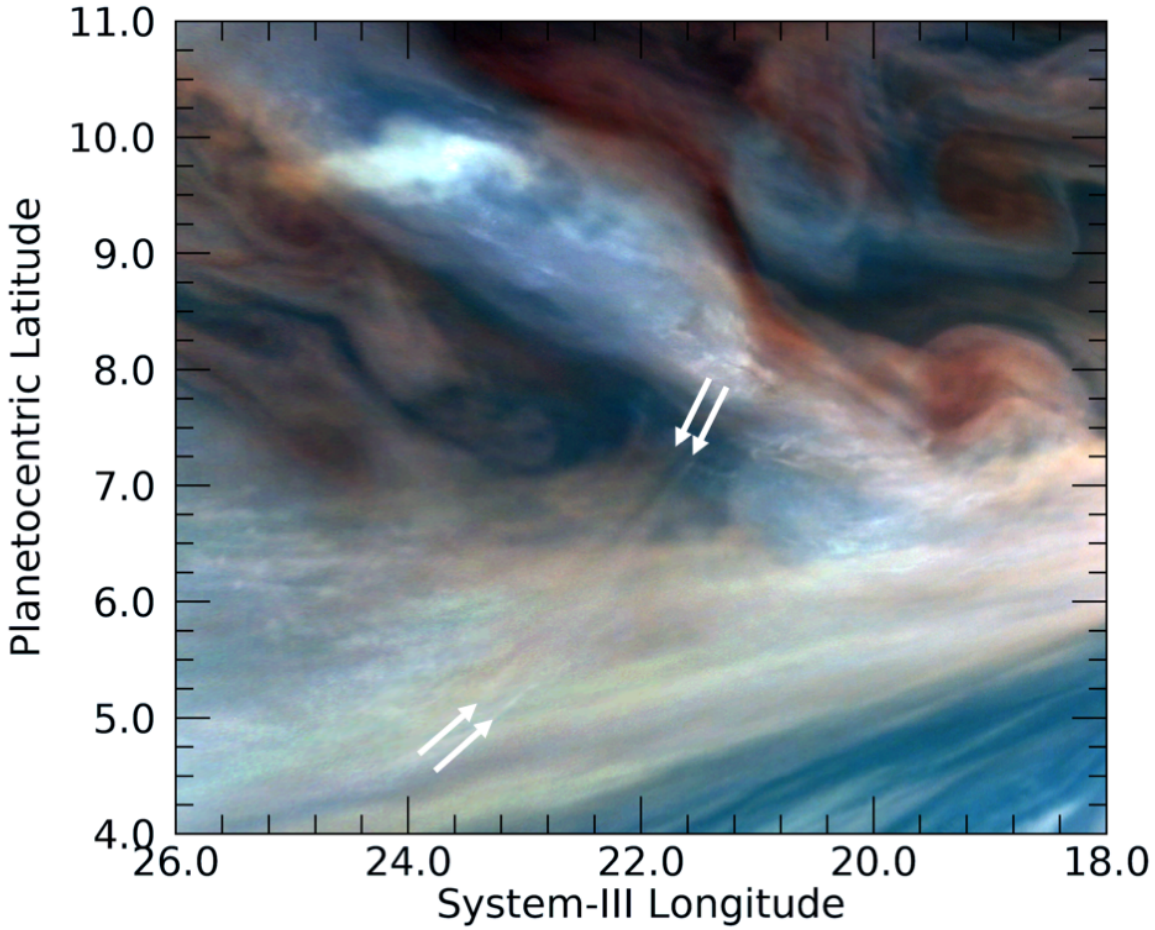

Figure PJ20_33. JNCE_2019043_20C00033_V01. Arrows denote a pair of bright curvilinear waves in the northern component of the Equatorial Zone. This image has also been unsharp-masked, as well as color-stretched, in order to make this feature more prominent.

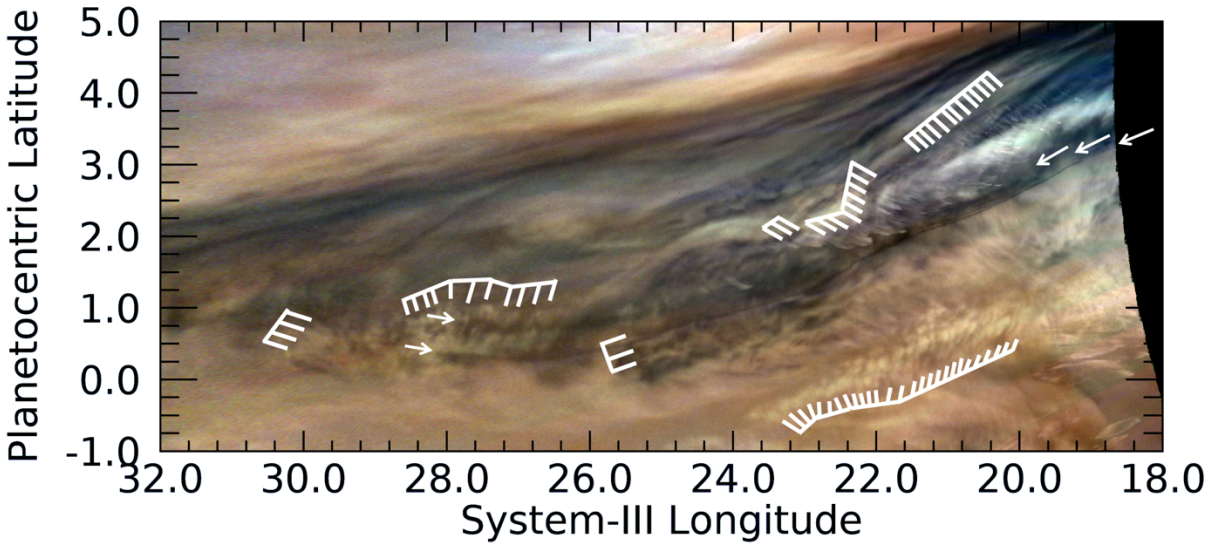

Figure PJ20_34a. JNCE_2019149_20C00034_V01. A wide variety of waves are detectable at this southern extension of a 5-µm hot spot "festoon", some of which are indicated by white gridlines. This is just south of (and slightly overlapping with) the area in Fig. PJ20_33. Three parallel lines, two of whose origins can be seen on their eastern end, are denoted by left-pointing arrows. Two can be seen out to the point denoted by the right-pointing arrow. (A version of this figure, indicating only the long, dark waves is shown in the Figure 7 of the main article. It also includes the area shown in Fig. PJ20_33.)

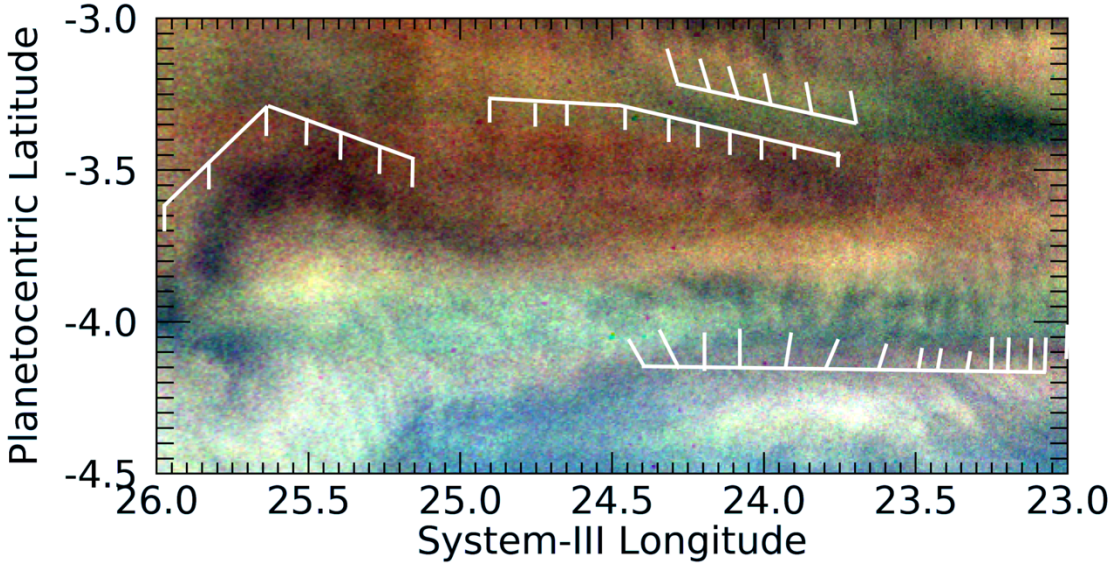

Figure PJ20_34b. JNCE_2019149_20C00034_V01. Long wave packets, some straight and some curved, and short wavefronts in the southern component of the Equatorial Zone. These are barely resolved above the noise.

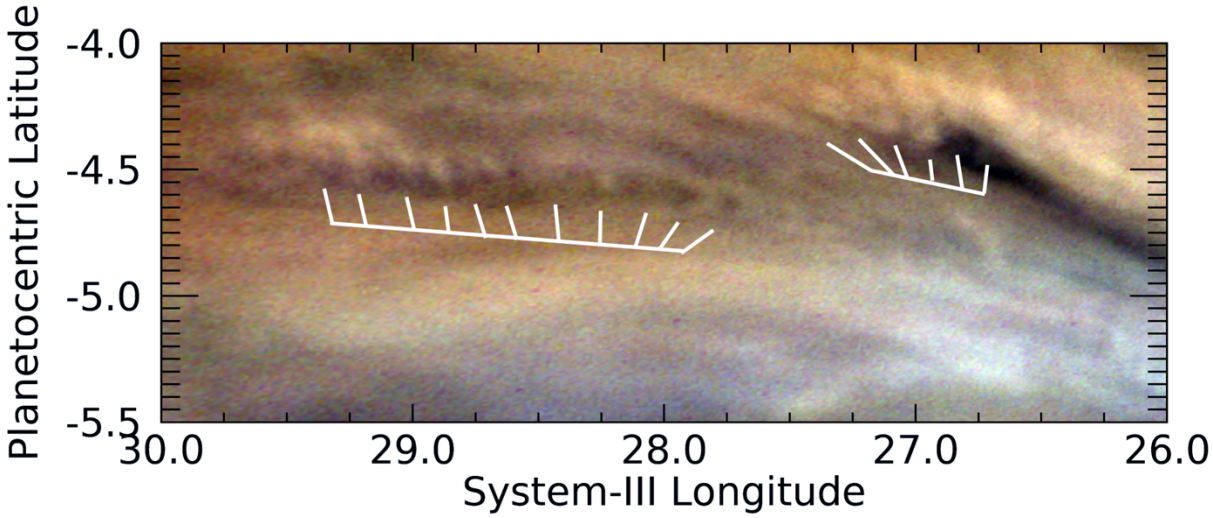

Figure PJ20_34c. JNCE_2019149_20C00034_V01. Long wave packets and short wave fronts just to the west of the area in Fig. PJ20_34b in the southern component of the Equatorial Zone.

.

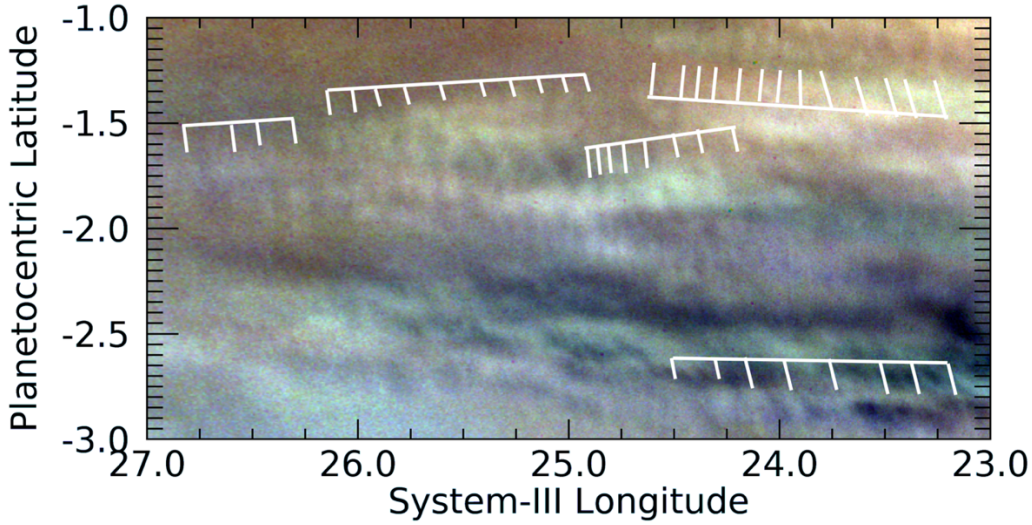

Figure PJ20_36. JNCE_2019149_20C00036_V01. Many, probably related, wave packets can be seen in this image, showing a region to the south of Figure PJ20_34b in the southern component of the Equatorial Zone.

2. Table of Measured Wave Properties

PJ	Image	No. of Waves	Mean System-III Longitude	Mean Planeto-centric Latitude	Length(km)	Width(km)	Mean Wave-length (km)	Tilt (deg.)
1	99	12	277.382	2.265	1443.019	172.21	131.184	99.162
3	109	3	186.553	25.643	294.498	243.237	147.249	81.644
3	109	4	185.569	30.624	923.487	669.582	307.829	76.658
3	109	3	186.971	29.661	566.545	747.226	283.272	68.168
3	109	3	185.081	23.09	723.737	435.96	361.869	69.137
3	111	18	188.947	1.971	1881.469	807.872	110.675	90.118
3	111	12	186.847	1.683	1159.12	249.21	105.375	68.986
3	111	7	186.353	-5.192	999.148	373.697	166.525	98.205
3	114	6	198.845	-15.06	974.176	237.979	194.835	99.958
3	114	17	196.482	-16.136	2647.844	331.13	165.49	93.179
3	114	7	198.92	-15.613	921.312	789.697	153.552	86.02
3	114	12	198.611	-17.186	2169.935	694.01	197.267	80.976
4	102	3	88.294	9.651	902.211	1256.075	451.106	107.759
4	103	3	94.586	14.396	308.766	318.943	154.383	60.98
4	103	3	94.297	13.761	324.722	502.262	162.361	71.651
4	103	3	93.46	14.415	403.787	608.365	201.894	84.274
4	103	3	93.665	13.285	405.154	382.57	202.577	127.897
4	103	3	94.542	12.856	425.525	484.863	212.763	62.579
4	103	26	95.135	11.974	912.752	74.937	36.51	50.39
4	103	6	94.029	11.497	145.531	34.184	29.106	75.165
4	104	15	96.778	1.804	2541.537	143.364	181.538	91.121
4	104	9	96.15	0.689	1321.284	398.368	165.16	83.882
4	104	10	95.172	-0.797	1409.911	387.944	156.657	101.797
4	104	5	96.304	2.999	1704.484	1225.699	426.121	25.082
5	107	3	8.978	0.119	229.063	868.076	114.531	123.29
5	107	6	8.006	0.289	1387.126	832.322	277.425	94.491
5	107	4	6.046	0.418	489.8	240.094	163.267	68.596
5	107	5	5.658	-0.143	426.439	249.488	106.61	101.447
5	107	5	6.343	-1.064	884.925	264.463	221.231	80.603
5	108	4	12.863	-17.475	693.047	986.53	231.016	98.382
6	115	14	321.429	2.556	1188.435	137.786	91.418	116.899
6	115	9	322.642	1.989	705.189	196.039	88.149	104.558
6	115	6	321.071	1.757	338.386	301.534	67.677	109.71
6	115	5	322	1.519	604.681	508.872	151.17	95.287
6	115	4	321.323	1.168	426.255	422.392	142.085	77.958
6	115	4	321.901	1.028	335.52	444.36	111.84	76.564

PJ	Image	No. of Waves	Mean System-III Longitude	Mean Planeto-centric Latitude	Length(km)	Width(km)	Mean Wave-length (km)	Tilt (deg.)
6	115	6	322.472	0.438	492.834	250.368	98.567	88.522
6	115	3	321.233	0.157	363.978	193.295	181.989	95.959
6	115	34	323.827	-4.392	5176.981	253.413	156.878	89.832
7	57	25	231.519	3.431	2149.808	155.682	89.575	97.524
7	57	6	230.81	3.367	690.467	198.183	138.093	59.358
7	57	6	232.003	2.812	1110.271	348.921	222.054	50.357
7	59	7	238.247	-15.837	432.642	233.899	72.107	77.713
7	59	9	237.785	-15.933	627.995	117.971	78.499	92.198
8	116	16	144.829	-2.34	1509.654	243.586	100.644	127.241
8	116	17	143.511	-3.157	1787.742	179.231	111.734	75.794
8	116	21	144.037	-4.932	1987.827	295.459	99.391	84.256
8	116	21	144.088	-5.147	2069.35	203.932	103.467	56.168
9	85	6	53.828	2.275	924.435	138.985	184.887	84.562
9	88	25	53.433	-3.743	5833.761	282.382	243.073	77.79
10	28	24	119.562	2.922	3474.263	216.488	151.055	75.458
10	30	4	127.448	-0.929	604.157	427.622	201.386	83.676
10	30	7	124.928	-1.629	848.834	310.479	141.472	101.49
10	30	6	125.289	-2.153	852.464	190.591	170.493	114.071
10	30	8	124.102	-2.212	940.918	204.228	134.417	95.875
10	30	6	126.57	-3.788	937.631	167.796	187.526	108.964
10	30	22	124.543	-3.286	3024.125	354.511	144.006	115.395
10	30	10	120.5	2.9	1449.339	170.546	161.038	81.646
11	20	4	38.728	3.542	943.652	647.318	314.551	88.002
11	20	27	34.794	2.649	4408.603	682	169.562	98.598
11	20	7	35.657	1.736	1764.856	309.633	294.143	113.921
11	20	9	31.974	1.769	1491.266	265.508	186.408	96.252
11	20	8	38.06	0.283	3829.259	1125.385	547.037	40.173
11	20	13	38.346	-3.49	2117.753	317.386	176.479	108.499
11	20	8	35.293	-3.376	2138.668	218.719	305.524	96.489
12	87	7	293.417	21.222	2909.154	255.532	484.859	102.626
12	87	7	293.236	19.862	1666.087	223.033	277.681	92.355
12	87	11	289.039	30.056	3785.29	273.643	378.529	95.127
12	90	24	299.804	-1.435	1128.009	421.205	49.044	54.886
12	90	27	301.906	-1.9	4751.839	441.836	182.763	126.704
12	90	19	300.76	-2.904	2448.543	319.937	136.03	113.474
12	90	7	302.942	-2.958	1338.207	164.908	223.035	87.4
12	90	20	302.722	-4.11	1613.772	238.806	84.935	96.995
12	90	8	301.668	-4.317	637.881	191.14	91.126	113.683
12	90	4	301.054	-4.41	320.594	362.324	106.865	140.122

PJ	Image	No. of Waves	Mean System-III Longitude	Mean Planeto-centric Latitude	Length(km)	Width(km)	Mean Wave-length (km)	Tilt (deg.)
12	90	19	299.754	1.497	2423.735	185.096	134.652	74.148
12	90	12	300.389	-4.964	339.877	62.197	30.898	88.094
12	86	4	293.736	32.989	391.608	279.77	130.536	108.477
12	86	4	294.254	32.354	129.47	45.525	43.157	71.254
12	86	3	294.093	32.436	98.921	35.222	49.46	93.528
12	86	4	294.048	31.969	333.476	162.809	111.159	73.657
12	86	5	289.186	34.167	543.441	588.21	135.86	118.294
12	86	4	289.889	33.25	286.03	390.818	95.343	100.068
12	86	4	288.518	32.49	412.983	303.692	137.661	113.29
12	86	4	289.04	32.228	310.823	1924.23	103.608	112.18
13	35	6	215.276	-1.576	1858.182	270.563	371.636	110.361
13	35	4	219.258	-1.642	574.782	513.442	191.594	95.481
13	35	11	220.172	-3.496	2421.856	387.182	242.186	76.368
13	35	13	216.56	-4.549	1777.015	547.982	148.085	117.934
13	35	10	214.632	-4.662	2421.237	627.054	269.026	80.995
13	35	5	221.562	-4.514	875.349	339.621	218.837	109.908
13	35	9	220.383	-4.975	1152.51	449.464	144.064	105.735
13	35	6	217.954	-4.669	1171.04	456.782	234.208	123.702
13	35	10	216.356	-4.66	1561.142	394.509	173.46	127.062
13	35	11	217.948	1.854	2298.255	569.749	229.825	68.474
13	35	8	216.275	3.031	1527.479	728.131	218.211	71.463
13	36	6	222.974	-19.671	1109.853	75.506	221.971	79.597
13	36	4	221.939	-19.349	561.63	61.602	187.21	96.425
14	25	5	251.918	17.322	650.708	587.883	162.677	94.755
14	25	3	250.69	17.585	421.489	632.1	210.745	93.616
14	25	4	252.245	11.935	324.728	499.564	108.243	70.096
14	25	3	251.308	12.168	447.855	202.059	223.928	60.536
14	25	4	255.706	6.426	982.47	2170.505	327.49	103.689
14	25	4	253.429	6.783	1454.911	1030.651	484.97	70.728
14	28	6	262.072	-3.774	1517.03	256.277	303.406	93.522
14	28	4	259.751	-3.71	982.385	263.487	327.462	101.81
14	28	10	260.933	-4.557	1290.465	148.077	143.385	90.445
14	28	26	258.247	-4.529	4657.869	199.372	186.315	105.635
14	28	12	258.918	-5.054	2566.661	188.049	233.333	114.391
14	28	10	256.575	-5.382	2060.62	213.151	228.958	112.454
14	28	15	256.225	-6.031	1592.849	177.736	113.775	111.925
14	28	9	256.585	0.19	1259.986	415.229	157.498	60.212
14	28	8	258.039	-0.628	1614.514	408.693	230.645	89.539
14	28	7	259.961	-0.921	1652.792	543.307	275.465	118.616

PJ	Image	No. of Waves	Mean System-III Longitude	Mean Planeto-centric Latitude	Length(km)	Width(km)	Mean Wave-length (km)	Tilt (deg.)
14	28	5	259.663	-1.764	1126.946	402.052	281.736	126.892
14	28	5	256.697	-2.599	673.578	321.226	168.395	106.665
14	28	5	259.574	-3.59	1361.59	524.393	340.397	104.43
14	28	5	256.579	-3.347	933.251	273.61	233.313	127.994
15	24	9	331.914	22.707	960.217	220.453	120.027	135.183
15	29	6	347.466	-1.968	646.667	138.13	129.333	120.011
15	29	4	346.416	-2.676	501.554	239.424	167.185	125.577
15	29	5	347.613	-2.431	874.555	238.801	218.639	127.489
15	29	5	348.354	-2.007	673.4	458.58	168.35	86.87
15	29	23	347.087	-2.158	2411.423	439.493	109.61	110.576
16	19	14	259.2	-1.522	2504.494	478.935	192.653	110.948
16	19	10	256.577	-1.549	984.525	204.968	109.392	121.085
16	19	20	257.432	-2.276	2920.95	342.477	153.734	115.726
16	19	7	259.324	-2.378	1213.656	440.933	202.276	142.979
16	19	9	259.717	-3.926	1179.97	285.391	147.496	79.546
16	19	7	257.911	-4.383	1094.132	299.279	182.355	91.506
16	19	6	256.964	-4.292	833.27	195.811	166.654	99.875
17	26	4	179.208	4.343	1122.757	936.228	374.252	59.367
17	26	3	177.695	3.835	674.735	702.42	337.368	64.35
17	26	3	183.029	1.393	737.103	1246.419	368.552	85.567
17	26	4	178.393	1.09	2952.355	1236.364	984.118	108.093
17	26	3	181.868	0.085	1221.945	1557.643	610.973	124.411
17	26	6	176.48	-1.774	2521.5	432.048	504.3	71.013
17	26	3	174.442	-2.483	442.05	557.92	221.025	92.303
17	26	12	167.233	-4.825	2988.772	289.961	271.707	108.014
17	26	6	171.684	2.758	993.482	436.89	198.696	68.842
17	24	4	165.336	11.971	1640.593	1148.641	546.864	151.326
18	34	13	231.486	16.339	1479.678	253.295	123.306	123.337
18	38	2	253.097	4.496	336.919	990.799	336.919	84.997
18	38	4	250.31	4.383	1496.148	532.825	498.716	45.971
18	38	5	248.654	4.062	739.615	679.922	184.904	89.373
18	38	6	252.512	2.733	1236.615	1510.135	247.323	96.184
18	38	3	257.468	2.311	1143.566	1282.511	571.783	56.123
18	38	4	255.324	1.714	1792.617	955.643	597.539	109.6
18	38	3	251.435	0.61	942.497	610.11	471.248	113.798
18	38	14	248.909	-0.224	1802.454	177.615	138.65	75.268
18	39	8	261.87	2.035	4251.799	2824.37	607.4	62.121
18	39	4	261.65	0.497	2291.342	1374.944	763.781	57.473
18	39	10	255.183	-3.943	2556.687	344.928	284.076	126.152

PJ	Image	No. of Waves	Mean System-III Longitude	Mean Planeto-centric Latitude	Length(km)	Width(km)	Mean Wave-length (km)	Tilt (deg.)
18	39	8	255.905	-4.389	944.952	190.706	134.993	142.088
20	26	5	4.886	51.174	565.415	121.206	141.354	117.71
20	26	10	4.839	51.074	756.77	85.297	84.086	123.479
20	26	5	-1.2	47.657	469.003	123.759	117.251	60.501
20	33	2	22.432	6.251	297.424	3411.668	297.424	111.493
20	34	18	20.579	3.497	1744.981	340.611	102.646	102.313
20	34	10	22.167	2.312	1343.764	371.925	149.307	98.188
20	34	4	23.04	1.943	444.653	357.695	148.218	138.013
20	34	3	19.992	2.717	242.401	3239.177	121.201	161.543
20	34	27	21.701	0.143	4547.541	366.203	174.905	89.789
20	34	11	27.589	0.8	2394.442	232.073	239.444	75.893
20	34	4	29.836	0.49	591.212	404.267	197.071	92.153
20	34	3	25.168	0.569	580.303	418.457	290.152	76.352
20	34	21	20.147	3.3	1741.801	344.499	87.09	102.735
20	36	6	24.082	-3.126	826.219	255.142	165.244	117.219
20	36	10	24.196	-3.513	1115.638	191.28	123.96	97.573
20	36	7	25.533	-3.826	1075.969	275.562	179.328	72.29
20	36	14	23.789	-4.003	1809.431	261.721	139.187	115.76
20	36	6	27.171	-4.299	1245.436	513.153	249.087	142.469
20	36	11	28.522	-4.579	2102.104	209.768	210.21	71.011
20	36	13	23.908	-1.115	1616.669	176.566	134.722	85.7
20	36	10	25.49	-1.543	1557.731	194.765	173.081	105.401
20	36	4	26.542	-1.818	645.828	357.096	215.276	107.029
20	36	8	24.525	-1.817	987.207	227.244	141.03	106.439
20	36	8	23.699	-2.856	1396.802	239.859	199.543	114.772